

- ¹ Regional Climate Group, Department of Earth Sciences, Göteborg University, Göteborg, Sweden
² Rossby Centre, Swedish Meteorological and Hydrological Institute (SMHI), Norrköping, Sweden
³ Environment Administration, City of Göteborg, Sweden
⁴ Urban Climate Group, Department of Earth Sciences, Göteborg University, Göteborg, Sweden
⁵ Road Climatology Group, Department of Earth Sciences, Göteborg University, Göteborg, Sweden

Evaluation of MM5 mesoscale model at local scale for air quality applications over the Swedish west coast: Influence of PBL and LSM parameterizations

J.-F. Miao¹, D. Chen¹, K. Wyser², K. Borne¹, J. Lindgren³, M. K. S. Strandvall⁴, S. Thorsson⁴, C. Achberger¹, E. Almkvist⁵

With 10 Figures

Received 23 March 2006; Accepted 22 March 2007
Published online: July 30, 2007 © Springer-Verlag 2007

Summary

The performance of MM5 mesoscale model (Version 3.6.3) using different planetary boundary layer (PBL) and land surface model (LSM) parameterizations is evaluated and compared using high temporal and spatial resolution GÖTE2001 campaign data at local scale (a few kilometers) over the Greater Göteborg area along the Swedish west coast during 7–20 May 2001. The focus is on impact of PBL and LSM parameterizations on simulated meteorological variables important for air quality applications such as global radiation, diurnal cycle of near-surface air temperature and wind, diurnal cycle intensity, near-surface vertical temperature gradient, nocturnal temperature inversion, boundary layer height, and low-level jet (LLJ). The model performance for daytime and nighttime and under different weather conditions is also discussed. The purpose is to examine the performance of the model using different PBL and LSM parameterizations at local scale in this area for its potential applications in air quality modeling. The results indicate that the influence of PBL and LSM parameterizations on simulated global radiation, diurnal cycle of near-surface air temperature and wind speed, diurnal

cycle intensity, vertical temperature gradient, nocturnal temperature inversion and PBL heights, which are critical parameters for air quality applications, is evident. Moreover, the intensity and location of LLJ are simulated well by all schemes, but there also exist some differences between simulated results by using different PBL and LSM schemes. Therefore, the choice of PBL and LSM parameterizations is important for MM5 applications to air quality studies.

1. Introduction

The PSU/NCAR fifth-generation Mesoscale Model (MM5; Grell et al. 1995) is a limited-area, non-hydrostatic, terrain-following sigma-coordinate primitive equation model designed to simulate or predict mesoscale atmospheric circulation, and has been increasingly used in operational numerical weather forecasting (e.g., Kotroni and Lagouvardos 2004; Zhong et al. 2005) and air quality studies (e.g., Grell et al. 2000; Chandrasekar et al. 2003; Jackson et al. 2006; Mao et al. 2006; Miao 2006; Miao et al. 2006; Pérez et al. 2006; Sokhi et al. 2006). The model provides users with

Correspondence: Junfeng Miao, Department of Earth Sciences, Göteborg University, P.O. Box 460, 405 30 Göteborg, Sweden (E-mail: junfeng@gvc.gu.se)

many options of physical process parameterization schemes for cumulus convection, microphysics, radiation, planetary boundary layer (PBL), and land surface process that are suitable for a wide range of applications. A number of studies have indicated that MM5-simulated results are dependent on the parameterization schemes chosen by users (e.g., Kotroni and Lagouvardos 2001; Xu and Small 2002; Zamora et al. 2003; Mandal et al. 2004; Zhang and Zheng 2004; Berg and Zhong 2005; Ratnam and Kumar 2005).

In air quality modeling, MM5 can be used to provide detailed information on global radiation, surface air temperature, humidity, wind, and atmospheric stability (Barna et al. 2000; Shafran et al. 2000; Hogrefe et al. 2001). The quality of the meteorological model output is critical to the success of the air quality modeling effort (Angevine and Mitchell 2001). For air quality applications, PBL simulations closely related to PBL schemes and land surface schemes are extremely important (Betts et al. 1997; Ku et al. 2001; Xiu and Pleim 2001; Zhang et al. 2001; Athanassiadis et al. 2002; Rao et al. 2003; Pino et al. 2004). Surface fluxes of heat, moisture, momentum, and short/long wave radiation are crucial because they are the primary factors driving the development of the turbulent boundary layer (Seaman 2000). For example, Shafran et al. (2000) compared the performance of two types of turbulence closures in a three-dimensional numerical investigation of an episode with poor air quality, and found that the Gayno-Seaman turbulence scheme more accurately predicts boundary layer depth and surface wind speeds, when compared to the Blackadar non-local closure scheme.

Previous studies have also indicated that the choice of PBL schemes in MM5 is crucial to the simulated results within the PBL (Braun and Tao 2000; Bright and Mullen 2002; Zhang and Zheng 2004; Berg and Zhong 2005; Pérez et al. 2006). Among these studies, PBL schemes are often used in coupling with a simple slab model. However, the simulated results using PBL scheme are expected to be dependent on its coupling with land surface parameterization schemes (Seaman 2000). During the MM5 development, two advanced land surface models (LSMs) were introduced into the MM5 modeling system, respectively (Xiu and Pleim 2001; Chen and Dudhia 2001a), and are under continuous improvement. Until today, only a few studies from the developers have

validated their respective LSM performances in MM5 against the observations (Xiu and Pleim 2001; Chen and Dudhia 2001b). The studies show some improvements in the results using the advanced LSMs as compared to using slab model, but more studies need to be undertaken to evaluate the importance of the LSM with higher model resolution.

In the past years, a lot of efforts were made to evaluate MM5 performances for various applications and over different areas (e.g., Shafran et al. 2000; Hanna and Yang 2001; Hogrefe et al. 2001; Zhong and Fast 2003; Kotroni and Lagouvardos 2004; Lee and Fernando 2004; Zhong et al. 2005) to build confidence in applying the model. Nevertheless, the model performance also usually differs from application to application, and from location to location (Cox et al. 1998), not only depends on choice of physical process parameterization schemes. These evaluation studies provide us with better understanding of model performance in physical process parameterizations and applications, as well as a helpful guide on how to apply the model for certain purposes. However, most evaluations of MM5 are at synoptic or regional scales. So far, only a few studies (e.g., Zhong and Fast 2003; Kotroni and Lagouvardos 2004; Lee and Fernando 2004; Zhong et al. 2005) concerned the model performance at local scale (a few kilometers of horizontal resolution). Also, no existing study of MM5 performance is found over the Swedish west coast. Thus, there is clearly a need to adopt a validated model to study the processes involved in shaping the local meteorological conditions.

The above mentioned reasons and limitations motivate this study, and the high-resolution spatial and temporal observational data available from GÖTE2001 campaign (Borne et al. 2005) make this study possible. This study aims at evaluating the performance of MM5 mesoscale model comprehensively using various PBL and land surface parameterizations at local scale over the Greater Göteborg area along the Swedish west coast. The emphasis is on the variables related to local climate and air quality applications (e.g., diurnal cycle of near-surface air temperature and wind, diurnal cycle intensity, daytime heating/nocturnal temperature inversion, vertical temperature gradient, and PBL height). The model's capability of reproducing LLJ is also examined.

2. PBL and LSM parameterizations used and model setup

The following PBL and LSM schemes in MM5 (Version 3.6.3) are chosen for evaluation in this study for two main considerations: (1) availability of coupling of PBL schemes and LSMs in the model, and (2) availability of the model output of near-surface (2-m) temperature without external computation/diagnosis.

2.1 PBL parameterizations

2.1.1 Blackadar PBL scheme

The Blackadar PBL scheme (Blackadar 1976; 1979; Zhang and Anthes 1982) is a commonly used PBL scheme in the MM5. It consists of a nocturnal module and a free convection module of turbulent mixing. In the nocturnal module, a first-order closure approach based on K theory is used to determine the turbulent fluxes, mixing is assumed to occur only between adjacent model layers (local scheme), and the PBL height is artificially set at the surface layer (top of the first model sigma layer); In the free convection module, a non-local approach is used where buoyant plumes of warm air are assumed to mix heat, moisture and momentum at every level of the mixed layer. The PBL height is diagnosed from the virtual potential temperature profiles and is taken as the height where the negative energy fluxes (downward heat fluxes due to overshooting) reach 20% of the total positive energy (upward heat fluxes due to surface heating).

2.1.2 Eta PBL scheme

The Eta PBL (Janjić 1990; 1994) scheme is based on an implementation of Mellor-Yamada (1974) level-2.5 scheme or a variant of 1.5-order closure model that includes a prognostic equation of the turbulent kinetic energy (TKE). Like other TKE closures, the non-local K approach is used. This scheme is used to forecast vertical mixing of horizontal wind, potential temperature and mixing ratio. The PBL height is diagnosed from the vertical profiles of the wind, potential temperature and specific humidity based on the critical bulk Richardson number.

2.1.3 MRF PBL scheme

The MRF PBL (Hong and Pan 1996) scheme is a first-order, non-local K scheme, which includes

countergradient transports of temperature and moisture that account for the contributions from large-scale eddies. The eddy diffusivity coefficient for momentum is a function of the friction velocity and the PBL height, and that for temperature and moisture is computed from the one for momentum based on the Prandtl number relationship. The PBL height is calculated based on the critical bulk Richardson number.

2.1.4 Pleim–Chang PBL scheme

The Pleim–Chang PBL scheme (Pleim and Chang 1992) is a derivative of the Blackadar PBL scheme, and is a non-local closure model referred to as the Asymmetrical Convective Model (ACM), which is designed to simulate rapid upward transport from the surface layer to all levels within the convective boundary layer by rising buoyant plumes and more gradual downward transport by broad slow compensatory subsidence (Pleim and Xiu 1995). The PBL height is estimated according to a bulk Richardson number (Ri_b) method. The top of the PBL is defined as the height at which Ri_b first equals the critical Richardson number.

Besides the references cited above, the reader is also directed to Braun and Tao (2000), Bright and Mullen (2002), Zhang and Zheng (2004), Fan and Sailor (2005), and Pérez et al. (2006) for further details and/or summary descriptions regarding the PBL schemes.

2.2 LSM parameterizations

2.2.1 SLAB LSM

The SLAB LSM, named in this study, consists of: (1) a five-layer soil temperature model (Dudhia 1996), and (2) a bucket soil moisture model (Manabe 1969). The model is used to predict the soil temperature in the five layers with thickness from top to bottom of 1, 2, 4, 8, and 16 cm, and keeps a budget of soil moisture allowing moisture availability to vary with time in response to rainfall and evaporation rates in this study.

2.2.2 Noah LSM

The Noah land surface model is used to predict soil moisture and temperature in four layers with thickness from top to bottom of 10, 30, 60, and 100 cm, as well as canopy moisture and water-

equivalent snow depth (Chen and Dudhia 2001a). It uses soil and vegetation types in handling evapotranspiration. The dominant vegetation type in each grid is selected to represent the grid vegetation characteristics when the model horizontal grid resolution is larger than $1 \text{ km} \times 1 \text{ km}$.

2.2.3 Pleim–Xiu LSM

The Pleim–Xiu LSM (Xiu and Pleim 2001) includes a surface model dealing with soil moisture and evaporation, and a non-local closure PBL model (i.e., aforementioned Pleim–Chang PBL scheme). It represents soil moisture and temperature in two layers (a 1-cm surface layer and a 1-m root zone layer), as well as canopy moisture, and handles soil surface, canopy and evapotranspiration moisture fluxes. It uses the percentage land use and soil data to aggregate soil and vegetation properties, rather than using a single dominant type. In this LSM scheme, the screen height is set to 1.5 m.

2.3 Model setup and initialization

The model is set up with four nested domains (D1, D2, D3, and D4) with horizontal grid spacing of 54, 18, 6, and 2-km, respectively (Fig. 1a). These four domains consist of 50×50 , 64×55 , 62×52 , and 40×46 horizontal grids (N–S direction by E–W direction), respectively. D1 has the size of $2700 \text{ km} \times 2700 \text{ km}$ covering Scandinavia, and is used to simulate the large scale meteorological conditions. The inner three domains with fine resolution are used to capture meso-scale and local scale features, of which the innermost domain (D4) is the area of interest (Fig. 1b). This area has remarkable sea-land contrast and urban–rural difference. All domains have 34 vertical levels and the model top is at 100 hPa. About 18 levels are within the lowest 2 km, and the lowest model level (half- σ level) is at about 10 m, which represents the average over the lowest 20 m above the surface.

The following physics options are used: Anthes-Kuo convection scheme in D1, Kain–Fritsch convection including shallow convection (KF2; Kain 2004) in D2–D4. Dudhia simple ice microphysics scheme (Dudhia 1989), Rapid Radiative Transfer Model (RRTM) longwave scheme (Mlawer et al. 1997), and Dudhia cloud-

Table 1. Summary of numerical experiment schemes

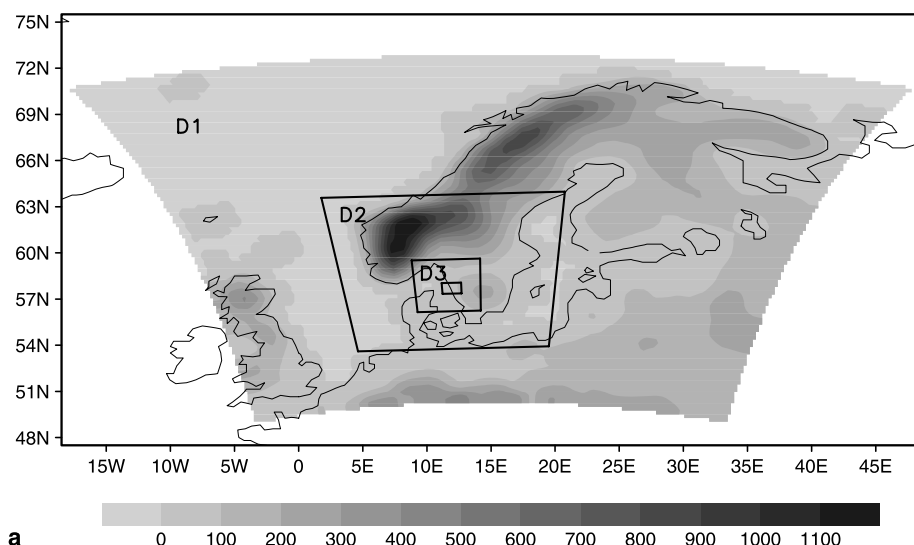
Experiment name	PBL parameterization ^a	LSM parameterization
BLKSLAB	Blackadar	SLAB
EtaSLAB	Eta	SLAB
MRFSLAB	MRF	SLAB
EtaNOAH	Eta	Noah
MRFNOAH	MRF	Noah
ACMPX	Pleim–Chang	Pleim–Xiu

^aMoist vertical diffusion is used in Blackadar, MRF and Pleim–Chang PBLs; Thermal roughness length uses Zilitinkevich formulation in Blackadar and MRF PBLs

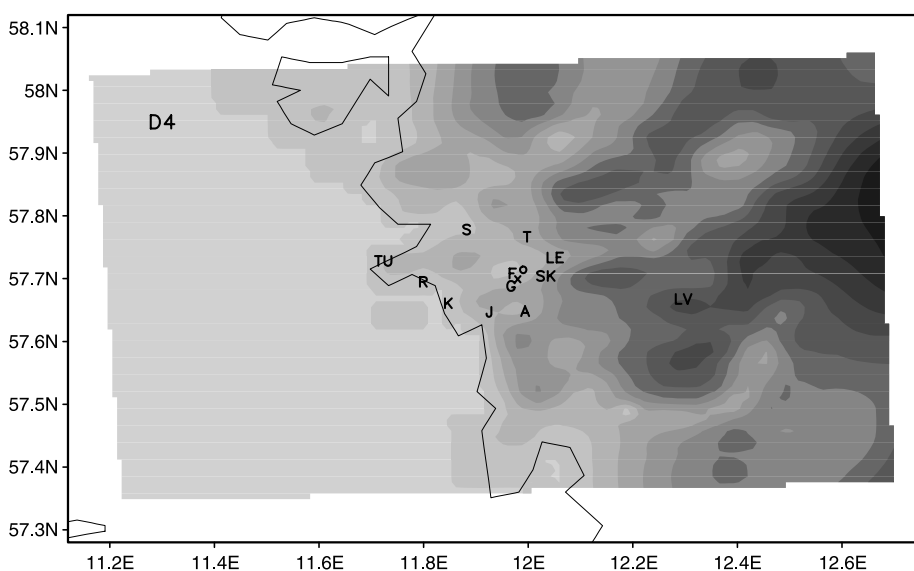
radiation shortwave scheme (Dudhia 1989) for all domains. Two-way nesting scheme is used, and no data assimilation is used in the model. These options are kept fixed in all numerical experiments summarized in Table 1 to examine the influence of different PBL and LSM parameterizations on the simulated results. In this study, Kain–Fritsch convection parameterization is applied in D4 with less than 5 km grid spacing for the reason that the scheme has been lately updated and also taken shallow convection into consideration (Kain 2004) for some potential improvements at higher resolutions.

The initial and boundary conditions used for all simulations were taken from the ECMWF operational analysis archive data with the spatial resolution of 0.5° by 0.5° and the temporal resolution of six hours. The model uses these discrete-time analyses by linearly interpolating them in time to the model time for lateral boundary conditions. The USGS 25-category land use data and terrain data, as well as global 17-category soil data are used. The topographical feature for the coarse domain (D1) with $54 \text{ km} \times 54 \text{ km}$ resolution is shown in Fig. 1a, while that for the innermost domain (D4) with $2 \text{ km} \times 2 \text{ km}$ is shown in Fig. 1b. As seen from Fig. 1b, the terrain height in D4 varies from a few meters near the coastal lines to about 200 m over the inland areas. Moreover, soil moisture is initialized for the LSMs using the ECMWF data.

The simulations are conducted from 0000 UTC 6 May 2001 to 2400 UTC 20 May 2001 with model output at intervals of an hour. The first day is discarded as spin-up and the remaining 14 days are analyzed. The latter period spans GÖTE2001 campaign (Borne et al. 2005).



a



b

Fig. 1. (a) Modeling domains and grid configuration.

Domains 1, 2, 3, and 4 (denoted by D1, D2, D3, and D4) have a horizontal grid spacing of 54, 18, 6, and 2 km, respectively. The innermost domain refers to D4. Shaded is model terrain (in meters) with 54-km grid resolution for D1; (b) Zooming-in D4 and model terrain (in meters) with 2-km grid resolution, as well as the locations of observational sites: Järnbrott (J), Åby (A), Femmanhuset (F), Lejonet (o), Tagene (T), Risholmen (R), GVC (G), Heden (x), Skatås (SK), Lemningsvallen (LE), Tumlehed (TU), Kanotföreningen (K), Säve (S), and Landvetter (LV)

3. GÖTE2001 observation and evaluation methods

The observational data used for model evaluation in this study are mainly from the GÖTE2001 field campaign (Borne et al. 2005), which was conducted in the Greater Göteborg area along the Swedish west coast in a 2-week period from 7 to 20 May 2001. During this period, the Swedish west coast was dominated by a high pressure system from 7 to 12 May 2001, and dominated by a low-pressure system from 13 to 20 May 2001.

One of the primary objectives of the field campaign was to collect an extensive dataset suitable

for validation of meteorological models applied over the Swedish west coast, and thus improve the understanding of meteorological processes responsible for the transport of air pollutants under different weather conditions. To this end, the campaign measured meteorological and air pollution variables descriptive for a broad range of the terrain characteristics (e.g., land use and topography) at local scale. Details about the field campaign can be found in Borne et al. (2005). In brief, Table 2 outlines the basic information about the field stations and the measured meteorological variables used only in this study, in which one routine weather station (Säve) and a

Table 2. Name, location and other information for the observational sites used in this study (Lat.: latitude, Lon.: longitude, Elev.: elevation), as well as the model terrain (TER) and dominant land use (LU) represented in 2-km resolution (D4) closest to the sites

Site name ^a	Lat. (°N)	Lon. (°E)	Elev. (m)	Measured variable ^c	Source ^d	TER (m)	LU
Järnbrott (3,73, 85,105) (16,56,105)	57.6472	11.9259	7	T , WS, WD	Miljo-	40	Urban
Åby	57.6483	11.9941	8	T_3 , WS ₁₀ , WD ₁₀	Miljo-	43	Urban
Femmanhuset	57.7085	11.9701	28 ^b	T_1 , WS ₅ , WD ₅	Miljo-	20	Urban
Lejonet	57.7149	11.9917	3	T_2 , WS ₁₀ , WD ₁₀ , R _{s↓}	Miljo-	24	Urban
Tagene	57.7670	11.9979	3	T_3 , WS ₁₀ , WD ₁₀	Miljo-	45	Crop
Risholmen	57.6950	11.7995	10	T_3 , WS ₃₅ , WD ₃₅	Miljo-	0	Water
GVC	57.6886	11.9663	85 ^b	T_2 , WS ₇ , WD ₇	RCCG	43	Urban
Heden	57.7019	11.9795	4	T_2 , WS ₁₀ , WD ₁₀	UCG	20	Urban
Skatås	57.7046	12.0339	65	WS ₁₀ , WD ₁₀	UCG	61	Urban
Lemningsvallen	57.7340	12.0517	10	WS ₁₀ , WD ₁₀	UCG	40	Urban
Tumlehed	57.7286	11.7241	2	WS ₁₀ , WD ₁₀	UCG	19	Crop
Kanotföreningen	57.6609	11.8476	9 ^b	WS ₂ , WD ₂	RCCG	0	Water
Säve	57.7786	11.8824	16	T_2 , SLP, CC	SMHI	18	Forest
Landvetter	57.6678	12.2963	169	RAOB	NOAA	136	Forest

^a Järnbrott is a mast site. 3, 73, 85, and 105 are the measurement height (m) for temperature, while 16, 56, and 105 for wind speed and wind direction; Säve is a routine weather station (SMHI), and Landvetter is a radiosounding (RAOB) station

^b Height of mounted measurement mast from the sea level to the roof. For Femmanhuset, the elevation is 3 m, and the building height is 25 m; For GVC, the elevation is 60 m, and the building height is 25 m; For Kanotföreningen, the elevation is 3 m, and the building height is 6 m

^c T : air temperature; WS: wind speed; WD: wind direction. Subscript represents the measured height above ground level (AGL) or above the roof; SLP: sea-level pressure; CC: cloud cover, which is measured in octas (0–8, 0 = clear, 8 = overcast); R_{s↓}: downward shortwave radiation (Global Radiation); RAOB: radiosounding; Hourly data for all sites except for Säve and Landvetter (3-hour time interval T_2 , SLP and CC at Säve, and 12-hour time interval RAOB at Landvetter)

^d Miljo-: Environment Administration, City of Göteborg; RCCG: Regional Climate Group, UCG: Urban Climate Group, Göteborg University; SMHI: Swedish Meteorological and Hydrological Institute

radiosounding station (Landvetter) are included for more data. Also, model terrain (topography) and land use data are presented in Table 2, and the locations of these observational sites are shown in Fig. 1b.

The model output at the closest gridpoint to observational site from D4 is used to compare with the observed results. The modeled near-surface air temperature and wind are not adjusted vertically to the measurement heights, although there are some differences between the model levels and the measurement heights. The reasons are as follows: (1) our concern emphasizes on the effects of different PBL and LSM parameterizations on simulated results, (2) there is also difference between model terrain height and actual terrain elevation (cf. Table 2), and (3) adjusting the temperature using a standard lapse rate (6.5 K km^{-1}) does not necessarily lead to an improvement in model skill (Cheng and Steenburgh 2005).

To quantitatively evaluate the model's performance, the following standard statistical measures over space and/or time are computed:

– Mean bias error:

$$\text{MBE} = \frac{1}{N} \sum_{i=1}^N \phi'_i;$$

– Root-mean-square-error:

$$\text{RMSE} = \left[\frac{1}{N-1} \sum_{i=1}^N \left(\phi'_i \right)^2 \right]^{1/2};$$

– Ratio of modeled (σ_{mod}) to observed (σ_{obs}) standard deviations:

$$\text{Ratio} = \frac{\sigma_{\text{mod}}}{\sigma_{\text{obs}}};$$

– Standard deviation of the difference between the modeled and observed variables:

$$\sigma_{\text{diff}} = \left[\frac{1}{N-1} \sum_{i=1}^N \left(\phi'_i - \text{MBE} \right)^2 \right]^{1/2};$$

- Correlation coefficient (R);
- Root-mean-square error for wind vector:

$$\text{RMSVE} = \left[\frac{1}{N-1} \sum_{i=1}^N (u_i'^2 + v_i'^2) \right]^{1/2},$$

where ϕ_i' is the departure of the modeled variables from the observed values at the i -th sampling point; u_i' and v_i' stand for the departure of horizontal wind components in X- and Y-direction, respectively. N is the total sampling over space and time ($N = m \times n$). σ_{mod} , σ_{obs} and R are conventional statistical parameters. For $N = m \times n$, m is numbers of spatial points, n is ones of observational/forecast hours (temporal points). If $m = 1$, the statistical measures are computed only over the temporal domain.

The above relevant formulas and methodologies can be found in Hogrefe et al. (2001), Taylor

(2001), Zhong and Fast (2003), and/or Zhong et al. (2005). Among these statistical parameters, MBE represents systematic errors which are usually caused by consistent misrepresentation of local properties (e.g., land use and topography) and/or physical mechanisms such as cumulus convection and radiation (Zhong et al. 2005); σ_{diff} indicates nonsystematic errors, representing the random error components caused by uncertainties in model initial and boundary conditions or in the observations (Zhong et al. 2005). σ_{diff} also contains a component of natural observed variability because the model value is an average over a grid volume, whereas the observed value is a discrete point measurement (Case et al. 2002); R quantifies pattern similarity, and σ_{mod} and σ_{obs} represent the variability of the modeled and observed variables, respectively.

Table 3. Statistical parameters of 3-hour sea-level pressure (SLP in hPa) modeled by different experiment schemes at Säve site

Statistics ^a	BLKSLAB	EtaSLAB	MRFSLAB	EtaNOAH	MRFNOAH	ACMPX
MBE	0.2	1.0	0.7	1.0	0.4	0.8
RMSE	0.8	1.8	1.3	1.6	1.1	1.3
σ_{diff}	0.8	1.2	1.1	1.2	1.1	1.0
Ratio	1.03	1.08	1.06	1.08	1.05	1.02
R	0.997	0.996	0.997	0.997	0.996	0.996

^a Based on 3-hour interval SLP data during the period of 7–20 May 2001 (sample number: $N = 112$)

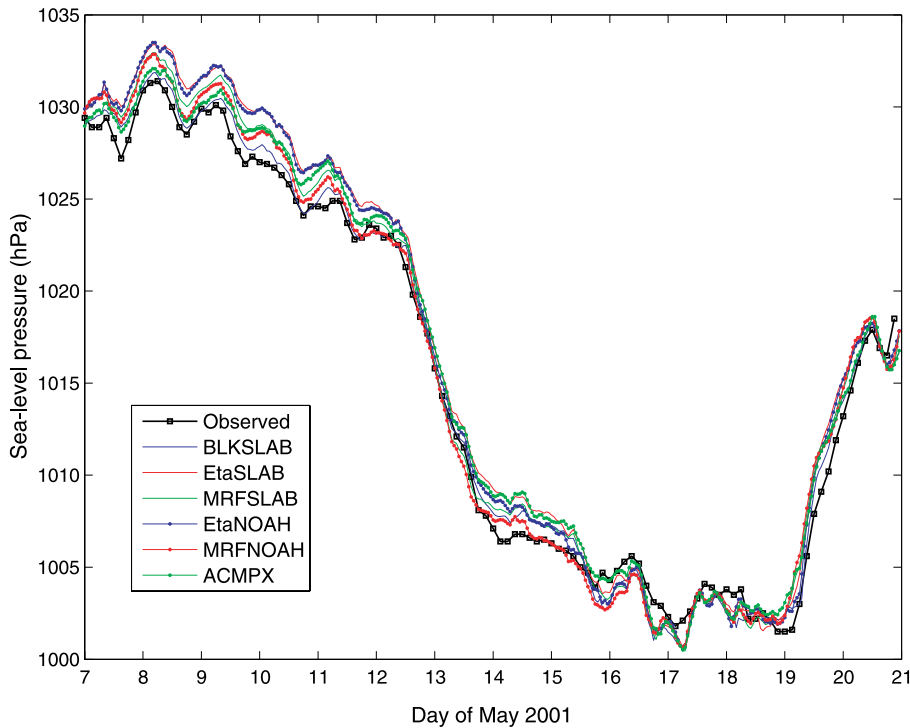


Fig. 2. Time series of modeled hourly sea-level pressure at the closest grid point to Säve site from D4 with 2-km grid resolution by different experiment schemes during the period from 0000 UTC 7 May to 2300 UTC 21 May 2001 (sample number $N = 336$). Observed sea-level pressure at Säve site (3-hour interval) is denoted by solid line with square

4. Results and discussion

4.1 Overall model performance

4.1.1 Sea-level pressure and solar radiation

The modeled sea-level pressure (SLP) using different PBL and LSM schemes at the closest grid to the Säve site is compared with the observation in Fig. 2. It is evident that all schemes predict the magnitude and temporal variations of the observed SLP well. The diurnal variation of SLP can also be simulated well. Statistical parameters of modeled SLP by different schemes are summarized in Table 3. BLKSLAB scheme shows

the best performance in reproducing the observed SLP, whereas EtaSLAB and EtaNOAH schemes show the largest difference from the observation compared to other schemes. The correlation coefficient between the modeled and observed SLP for all schemes is very high, ranging from 0.996 to 0.997, indicating that all schemes reproduce the observed trends in SLP accurately. It is interesting to see from Fig. 2 that the observed SLP is systematically lower than all model runs for the first few days. In the model, SLP is a diagnosed variable, not a predicted one. It is calculated by using other variables such as terrain height, temperature at the lowest model level, pressure at the

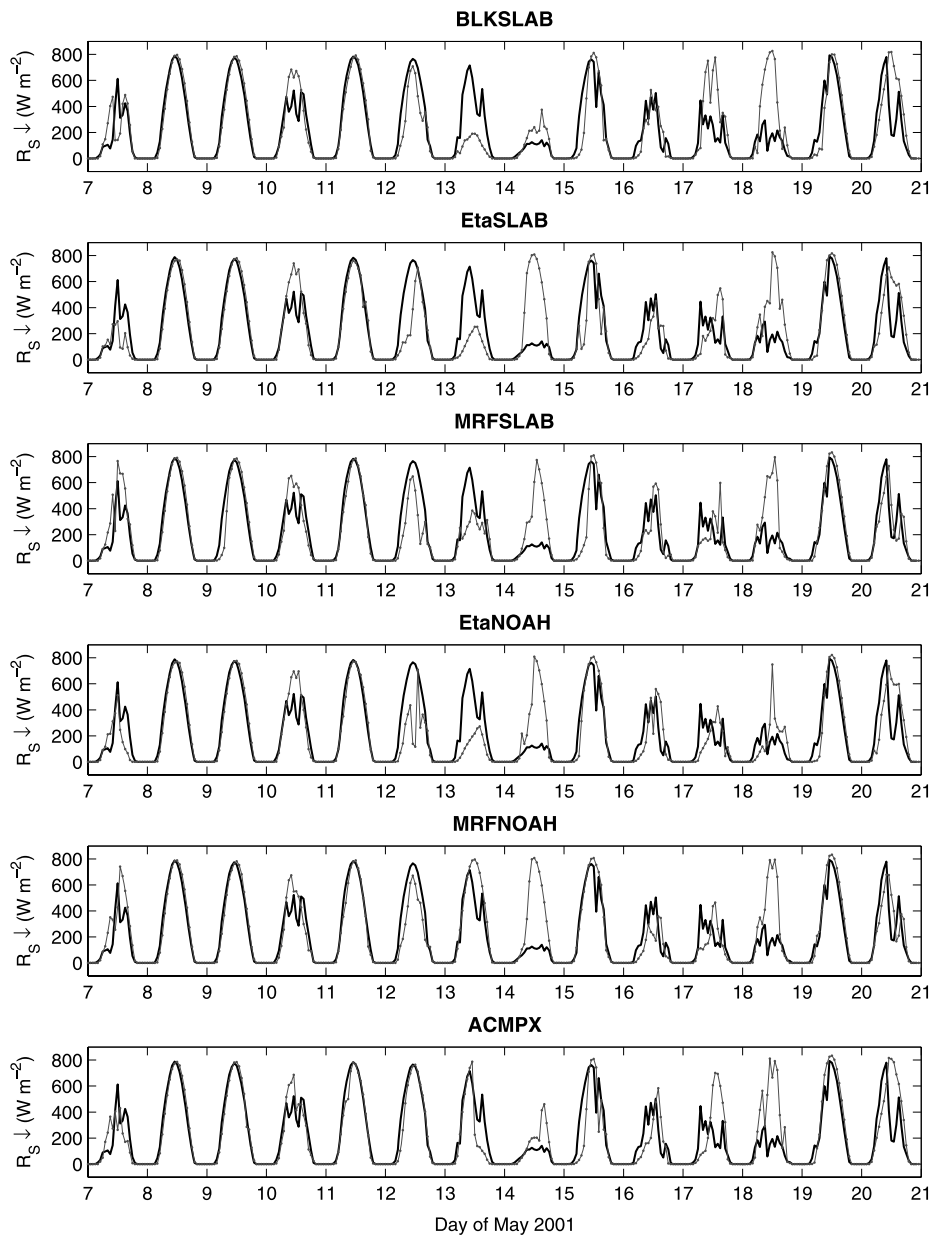


Fig. 3. Time series of modeled hourly downward solar radiation at the closest grid point to Lejonet site from D4 with 2-km grid resolution by different experiment schemes during the period from 0000 UTC 7 May to 2300 UTC 20 May 2001 (sample number $N = 336$). Observed hourly downward solar radiation at Lejonet site is denoted by thick solid line in each plot for comparison

model top, and perturbation pressure at the lowest model level. Therefore, the errors in the other modeled variables (e.g., air temperature) would cause the errors in the calculated SLP. What seen from Fig. 2 shows that the model has a systematic error in the variables used in calculating the SLP in the beginning of the simulation. This in turn indicates that there are still some spin-off effects in the first few days.

Solar radiation is the primary forcing to surface climate and PBL dynamics, so its evaluation is crucial to comparing the model performance using different PBL and LSM schemes. Figure 3 shows hourly variation of observed and modeled downward solar radiation ($R_{s\downarrow}$) by different PBL and LSM schemes at the Lejonet site. On the whole, $R_{s\downarrow}$ is simulated reasonably well with all experiment schemes when compared to the observations. However, the model performance in $R_{s\downarrow}$ also depends on weather conditions to a larger extent. To clarify the effects of weather conditions on the model performance, the observed cloud cover at the Säve site is used to classify the

weather conditions into three groups: (1) clear days, (2) semi-cloudy days, and (3) cloudy days, according to Svensson and Eliasson (2002). On the basis of this classification, the statistical parameters are computed, and presented in Table 4. All schemes can simulate $R_{s\downarrow}$ fairly well on clear sky days, but overestimate it on cloudy days. The latter implies that the shortwave absorption and scattering by clouds is insufficiently represented by the model.

4.1.2 Near-surface air temperature and wind

An examination of near-surface air temperature and wind is important for model performance because these quantities reflect the nature of the local thermal circulation influenced by mesoscale forcing, and govern contaminant distributions in air quality models (Lee and Fernando 2004). The near-surface observational temperature data from 8 sites and wind data from 12 sites in Table 2 and Fig. 1b are used. Performance measures of the hourly data are presented in Table 5, while those

Table 4. Statistical parameters of hourly downward solar radiation ($W m^{-2}$) modeled by different experiment schemes^a at Lejonet site

Weather group ^b	Statistics ^c	BS	ES	MS	EN	MN	AP
All days (7–20 May 2001)	MBE	9	2	2	−10	31	15
	RMSE	192	208	181	184	177	174
	σ_{diff}	192	208	181	184	174	173
	Ratio	1.09	1.07	1.05	1.06	1.10	1.10
	R	0.73	0.68	0.75	0.75	0.79	0.79
Clear days (8, 9, 11, and 15 May 2001)	MBE	−15	−21	−38	1	−3	−31
	RMSE	108	113	136	77	67	118
	σ_{diff}	107	111	131	77	66	114
	Ratio	1.06	1.02	1.07	1.05	1.04	1.03
	R	0.94	0.93	0.90	0.97	0.98	0.92
Semi-cloudy days (10, 12, 13, 19, 20 May 2001)	MBE	−47	−47	−48	−63	4	6
	RMSE	210	215	168	224	147	163
	σ_{diff}	204	209	161	215	147	163
	Ratio	1.06	1.04	0.94	1.01	1.07	1.14
	R	0.69	0.67	0.78	0.64	0.84	0.83
Cloudy days (7, 14, 16–18 May 2001)	MBE	84	71	84	35	85	60
	RMSE	224	256	223	201	250	219
	σ_{diff}	208	246	206	198	236	210
	Ratio	1.70	1.74	1.73	1.47	1.78	1.60
	R	0.48	0.25	0.51	0.37	0.35	0.39

^a BS: BLKSLAB, ES: EtaSLAB, MS: MRFSLAB, EN: EtaNOAH, MN: MRFNOAH, AP: ACMPX

^b Classified according to observed daily mean cloud cover at Säve site: *Clear* (0–2 octas), *Semi-cloudy* (3–5 octas), and *Cloudy* (6–8 octas) (cf. Svensson and Eliasson 2002)

^c Based on hourly data for the daytime during the respective period. Sample number: $N = 71$ for *Clear days*, 90 for *Semi-cloudy days*, 89 for *Cloudy days*, and 250 for *All days*, respectively

Table 5. Statistical parameters of hourly near-surface air temperature and wind modeled by different experiment schemes^a

Statistics ^b	Time	Temperature (°C)						Wind ^c (m s ⁻¹)					
		BS	ES	MS	EN	MN	AP	BS	ES	MS	EN	MN	AP
MBE	All	-0.1	-0.9	-0.5	-1.1	-0.6	0.2	1.1	0.9	0.4	0.8	0.4	1.4
	Day	-0.4	-1.2	-0.7	-1.3	-0.5	-0.1	0.8	0.8	0.2	0.7	0.2	1.3
	Night	0.7	0.1	0.2	-0.6	-1.0	1.1	1.9	1.3	1.0	1.2	1.1	1.7
RMSE	All	2.4	2.6	2.7	2.7	2.7	2.3	2.5	2.0	2.1	2.0	2.1	2.5
	Day	2.6	2.8	2.9	2.9	2.8	2.4	2.4	1.9	2.1	1.9	2.1	2.4
	Night	1.9	1.9	2.0	2.3	2.4	2.1	2.8	2.2	2.1	2.2	2.1	2.7
σ_{diff}	All	2.4	2.5	2.6	2.5	2.6	2.3	2.2	1.8	2.1	1.8	2.0	2.1
	Day	2.5	2.5	2.8	2.5	2.7	2.4	2.2	1.8	2.1	1.8	2.1	2.0
	Night	1.8	1.9	2.0	2.2	2.2	1.8	2.0	1.8	1.8	1.8	1.8	2.1
Ratio	All	0.78	0.80	0.81	0.92	1.00	0.79	1.23	1.08	1.07	1.07	1.03	1.28
	Day	0.79	0.81	0.81	0.92	0.95	0.83	1.31	1.10	1.19	1.10	1.15	1.32
	Night	0.86	0.95	0.92	1.06	1.17	0.68	1.17	1.12	0.83	1.07	0.82	1.28
R	All	0.79	0.79	0.76	0.79	0.79	0.81	0.52	0.63	0.50	0.61	0.49	0.61
	Day	0.78	0.78	0.74	0.79	0.77	0.81	0.53	0.61	0.50	0.60	0.50	0.60
	Night	0.63	0.60	0.58	0.54	0.58	0.59	0.57	0.64	0.50	0.62	0.52	0.60
RMSVE	All	-	-	-	-	-	-	3.6	3.4	3.2	3.3	3.1	3.7
	Day	-	-	-	-	-	-	3.7	3.5	3.3	3.4	3.2	3.8
	Night	-	-	-	-	-	-	3.4	2.9	2.8	2.9	2.8	3.3

^a Abbreviation for experiment scheme name: same as in Table 4

^b Based on hourly data during the period of 7–19 May 2001. Sample number: $N = m \times n$; $n = 311$ for all hours ('All'), 232 for day hours ('Day'), and 79 for night hours ('Night'); $m = 8$ (sites) for temperature, while $m = 12$ for wind

^c Statistical parameters but RMSVE are only for wind speed

Table 6. Statistical parameters of daily maximum and minimum near-surface air temperature (T_{max} , T_{min}) and wind speed (WS_{max} , WS_{min}) modeled by different experiment schemes^a

Statistics ^b	BS	ES	MS	EN	MN	AP	BS	ES	MS	EN	MN	AP
	T_{max} (°C)						T_{min} (°C)					
MBE	-0.9	-1.4	-0.8	-1.1	-0.1	-0.1	0.7	0.2	0.2	-1.1	-1.3	1.7
RMSE	2.7	2.9	2.8	2.7	2.7	2.2	1.9	1.8	1.8	2.1	2.3	2.6
σ_{diff}	2.5	2.6	2.7	2.5	2.7	2.2	1.7	1.8	1.8	1.9	1.9	2.0
Ratio	0.65	0.64	0.56	0.74	0.63	0.73	0.95	1.04	1.07	1.17	1.23	0.67
R	0.74	0.72	0.69	0.74	0.69	0.82	0.62	0.63	0.65	0.66	0.68	0.36
	WS_{max} (m s ⁻¹)						WS_{min} (m s ⁻¹)					
MBE	1.1	0.7	0.2	0.6	0.1	1.5	0.9	0.8	0.5	0.6	0.5	0.9
RMSE	2.2	1.8	1.8	1.8	1.8	2.6	2.1	1.6	1.6	1.5	1.5	1.8
σ_{diff}	1.9	1.7	1.8	1.7	1.8	2.1	1.9	1.3	1.5	1.3	1.4	1.5
Ratio	1.23	1.15	1.19	1.20	1.10	1.50	1.64	1.16	1.17	1.14	1.15	1.26
R	0.66	0.71	0.67	0.71	0.67	0.73	0.40	0.50	0.38	0.48	0.47	0.41

^a Abbreviation for experiment scheme name: same as in Table 4

^b Based on daily data during the period of 7–19 May 2001. Sample number: $N = m \times n$; $n = 13$ for all days; $m = 8$ (sites) for temperature, and $m = 12$ for wind

of daily maximum and minimum data are summarized in Table 6.

As seen from Table 5, the modeled near-surface air temperature has a cold bias during the day and a warm bias during the night for BLKSLAB,

EtaSLAB and MRFSLAB schemes, yielding a small overall cold bias. For EtaNOAH and MRFNOAH schemes, the modeled near-surface air temperature has a cold bias during both daytime and nighttime, resulting in an overall cold

bias. ACMPX scheme predicts fairly well the near-surface air temperature overall, but overestimates it by 1.1 °C during the nighttime. The RMSE and σ_{diff} suggest that model performance is better during the nighttime than during the daytime for all schemes. The model predicts lower variability during the daytime than during the nighttime for all schemes but ACMPX, while ACMPX scheme has a much lower variability during the nighttime. Also, all schemes underestimate the variability during both daytime and nighttime except for EtaNOAH and MRFNOAH schemes during the nighttime. Further, the model has higher correlation during the daytime than during the nighttime for all schemes. For the modeled near-surface wind speed, the model has a positive overall bias ranging from 0.4 to 1.4 m s⁻¹ for all schemes (Table 5), overestimating 15–45%. The bias is larger during the nighttime than during the daytime. Other statistical measures show some slight differences among all schemes. RMSE of wind speed indicates a little bigger error during the nighttime than during the daytime for all schemes, whereas the RMSVE considering both wind speed and wind direction indicates that the error is a little smaller during the nighttime than during the daytime for

all schemes. Compared to the modeled near-surface air temperature, the modeled near-surface wind displays a lower correlation with the observations overall. Furthermore, the MBE and σ_{diff} of near-surface air temperature during the nighttime for ACMPX scheme are comparable in magnitudes, indicating that the systematic and nonsystematic errors contribute more or less equally to the total error, represented by RMSE. It is also true for the near-surface wind during the nighttime for all schemes.

Table 6 shows that the predicted daily maximum temperature has a cold bias for all schemes, and the predicted minimum temperature has a cold bias for EtaNOAH and MRFNOAH schemes, but has a warm bias for other schemes. Of all schemes, ACMPX displays the biggest warm bias (1.7 °C) and the smallest variability for minimum temperature. It is also seen that different schemes show different performance, especially in MBE and Ratio. Table 6 also shows that all schemes have positive bias of both the maximum and minimum wind speeds, ranging from 0.1 to 1.5 m s⁻¹ for maximum wind speed, and from 0.5 to 0.9 m s⁻¹ for minimum wind speed. All statistical parameters but R show the poorest performance for ACMPX scheme in predict-

Table 7. Statistical parameters of hourly near-surface air temperature and wind modeled by different experiment schemes^a for the first and second weeks^b

Statistics ^c	Time	Temperature (°C)						Wind ^d (m s ⁻¹)					
		BS	ES	MS	EN	MN	AP	BS	ES	MS	EN	MN	AP
MBE	W1	-1.0	-1.9	-1.8	-2.3	-1.9	0.2	0.6	0.6	-0.1	0.6	-0.1	0.9
	W2	0.6	0.0	0.7	-0.2	0.5	0.2	1.6	1.2	0.8	1.0	0.8	1.8
RMSE	W1	2.8	3.2	3.2	3.4	3.2	2.7	2.0	1.7	1.9	1.7	2.0	1.9
	W2	2.0	1.9	2.1	2.0	2.2	2.0	2.8	2.3	2.2	2.2	2.2	2.9
σ_{diff}	W1	2.6	2.6	2.7	2.5	2.5	2.7	2.0	1.6	1.9	1.6	2.0	1.7
	W2	1.9	1.9	1.9	2.0	2.1	2.0	2.3	1.9	2.1	1.9	2.0	2.2
Ratio	W1	0.79	0.82	0.82	0.96	0.98	0.72	0.94	0.89	0.91	0.88	0.92	0.90
	W2	0.89	0.93	0.97	1.00	1.26	0.89	1.27	1.11	1.05	1.12	0.99	1.36
R	W1	0.84	0.84	0.83	0.86	0.86	0.85	0.27	0.49	0.25	0.46	0.26	0.41
	W2	0.67	0.68	0.69	0.70	0.74	0.65	0.58	0.66	0.56	0.65	0.55	0.66
RMSVE	W1	-	-	-	-	-	-	3.2	3.1	2.9	3.1	2.8	3.2
	W2	-	-	-	-	-	-	4.0	3.5	3.4	3.4	3.4	4.1

^a Abbreviation for experiment scheme name: same as in Table 4

^b The first week ('W1'): 0000 UTC 7 May to 2400 UTC 12 May 2001 ($n = 144$), the second week ('W2'): 0000 UTC 13 May to 2200 UTC 19 May 2001 ($n = 167$)

^c Based on hourly data. Sample number: $N = m \times n$; $n = 144$ for W1, and $n = 167$ for W2; For temperature, $m = 8$, while for wind, $m = 12$ (sites)

^d Statistical parameters but RMSVE are only for wind speed

ing maximum wind speed, and for BLKSLAB scheme in predicting minimum wind speed. Also, all statistical parameters show that the performance of BLKSLAB scheme in predicting maximum wind speed is next to the worst (ACMPX), while all statistical parameters but R show that the performance of ACMPX scheme in predicting minimum wind speed is next to the worst (BLKSLAB).

It is clearly seen that the differences in modeled near-surface air temperature and wind, as well as daily maximum and minimum temperature and wind among using different PBL and LSM parameterizations are evident. This implies that the model performance to some extent depends on choice of PBL and LSM parameterizations.

In previous evaluation studies of near-surface air temperature and wind at local scale, only a few combination schemes of PBL and LSM parameterizations in MM5 were involved, e.g., BLKSLAB (Hanna and Yang 2001; Zhong and Fast 2003), EtaSLAB (Zhong et al. 2005), and MRFSLAB (Zhong and Fast 2003), while the other schemes such as EtaNOAH, MRFNOAH, and ACMPX were seldom evaluated. To our knowledge, the evaluation for MRFNOAH and ACMPX was carried out only by the developers of Noah LSM (Chen and Dudhia 2001b) and PX LSM (Xiu and Pleim 2001), respectively. The above results for BLKSLAB, EtaSLAB and MRFSLAB schemes are consistent with those from previous studies (Zhong and Fast 2003;

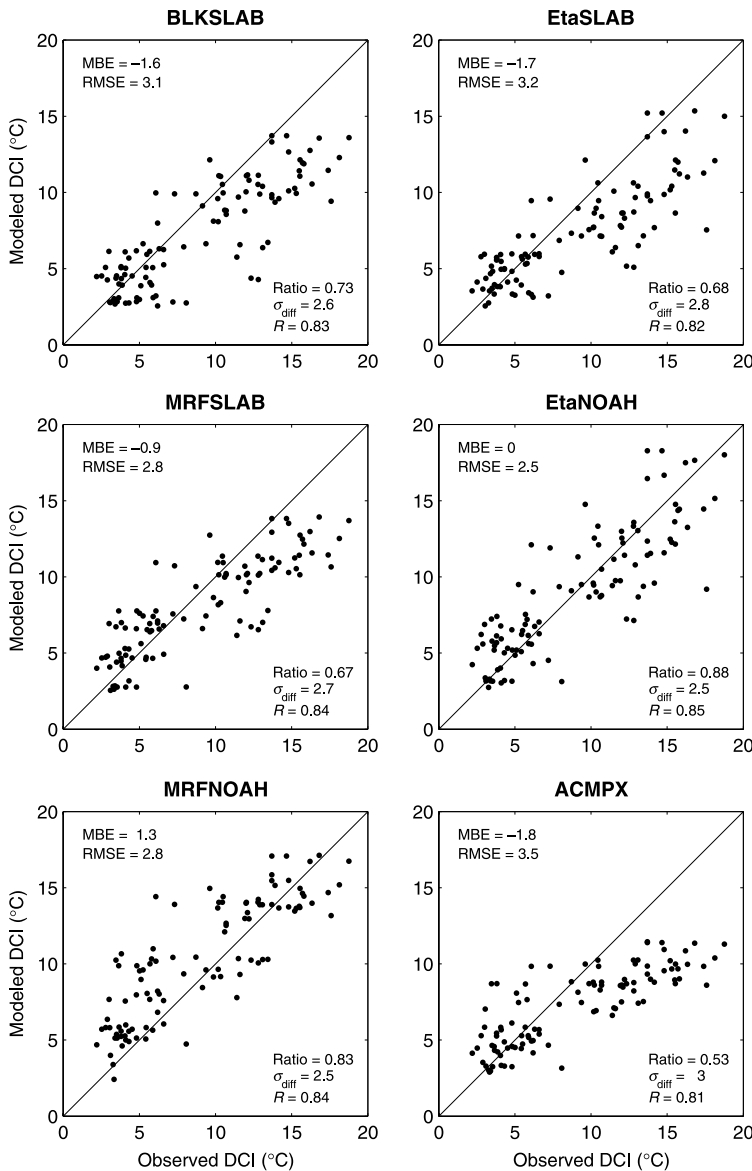


Fig. 4. Scatterplot of observed versus modeled diurnal cycle intensity (DCI) by different experiment schemes (cf. text for DCI definition). The results are based on 8 sites for measuring (hourly) near-surface air temperature (cf. Table 2) during the period from 7–19 May 2001 (sample number $N=104$). The statistical parameters are presented within the plot

Zhong et al. 2005), while those for other schemes such as EtaNOAH, MRFNOAH and ACMPX are quite new. It is also noted that PBL schemes are often used together with SLAB LSM, and less used with Noah LSM and PX LSM in the past evaluation studies of the MM5 model.

The above statistical evaluation was performed for the 2-week period. During this period, the synoptic conditions for the first week distinguish differently from those for the second week. Also, many previous statistical studies for evaluation on near-surface air temperature and wind are limited within a few days, and in most cases the weather conditions are characterized by clear skies and light winds. In this study, to examine the model performance under different weather

conditions, statistical parameters of near-surface hourly temperature and wind are computed for the first week period (dominated by high-pressure system, and characterized mainly by clear skies) and the second week period (dominated by low-pressure system, and characterized mainly by cloudy or rainy days), separately (Table 7). The results indicate that all schemes but ACMPX have a cold bias of 1.0 to 2.3 °C for near-surface air temperature for the first week, while ACMPX scheme has a very small warm bias (0.2 °C). Compared to the first week, the bias of near-surface air temperature for all schemes is relatively small (−0.2 to 0.7 °C). Both RMSE and σ_{diff} of near-surface air temperature for all schemes are consistently higher for the first week than for the

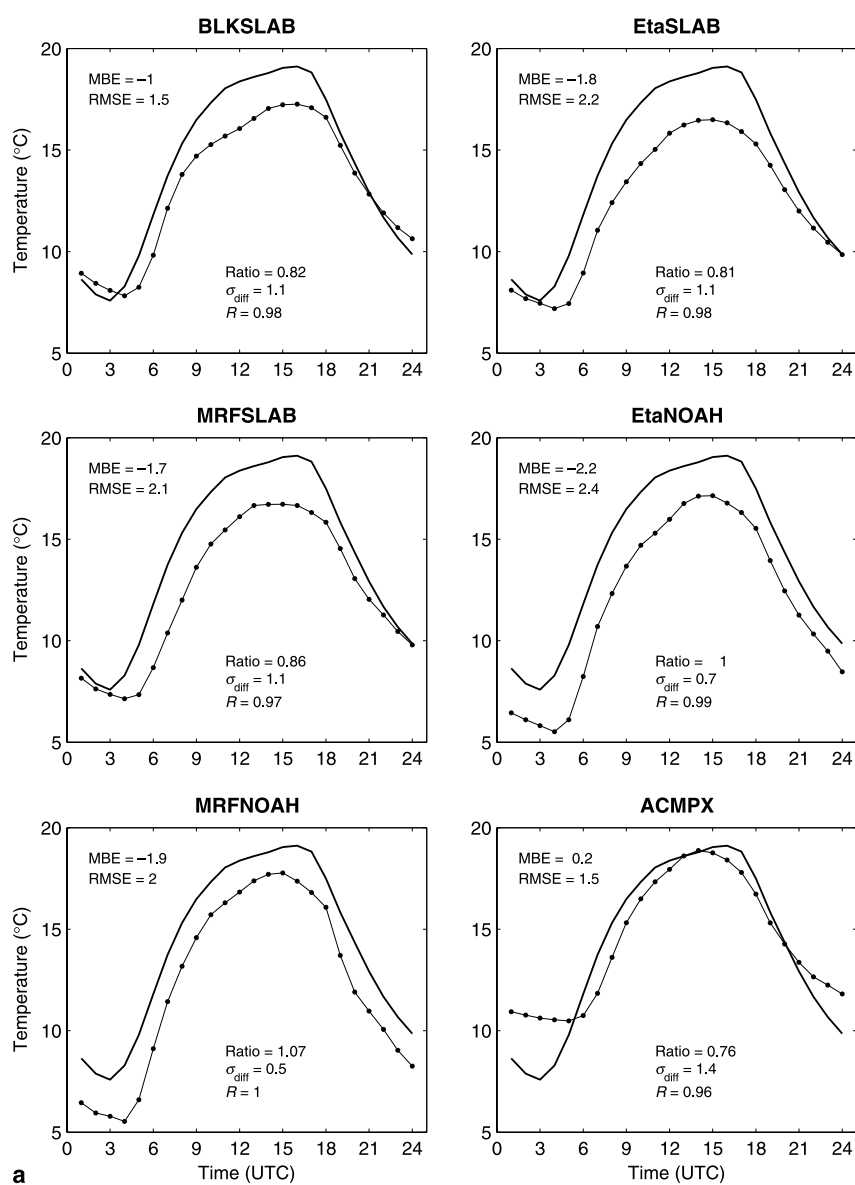


Fig. 5. Observed and modeled diurnal cycle of near-surface air temperature averaged spatially over 8 sites for first week (a) and second week (b). Observed diurnal cycle (solid thick line) is included in each plot for comparison. Diurnal cycle is based on the mean of hourly data for 7–12 May (the first week) and for 13–19 May (the second week), respectively. The statistical parameters are presented within the plot. Note that: 7–12 May is dominated by anti-cyclone (“High-Pressure System”), and mainly characterized as clear-sky days, while 13–19 May by cyclone (“Low-Pressure System”), and as cloudy or rainy days

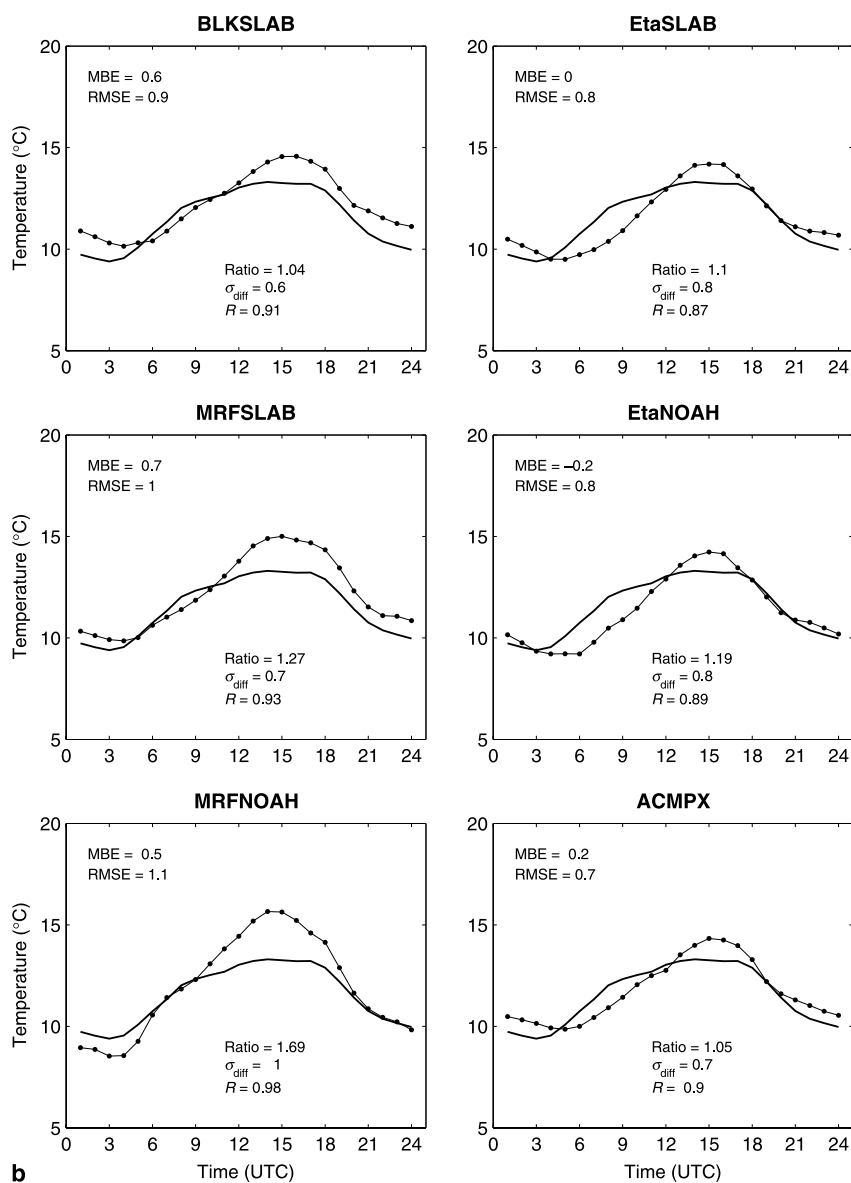


Fig. 5 (continued)

second week. This suggests that the model has better performance in predicting near-surface air temperature for the second week. For the near-surface wind, all statistical parameters but R indicate that all schemes reproduce the observations better for the first week than for the second week. However, the correlation coefficient R of near-surface air temperature for the first week is higher than that for the second week, while that of near-surface wind is just opposite.

The above different behaviors of near-surface air temperature and wind between the first week and the second week can be partly explained by the fact that local circulation plays a more important role during the first week, while synoptic scale weather dominates during the second week.

Under the high pressure system, the temperature shows high variability, while the wind speed displays small variability. On the other hand, under the low pressure system, the wind shows high variability, while the temperature displays small variability.

4.2 Diurnal heating and diurnal cycle

Local-scale circulations are driven by the heating contrast across the coastline or land use boundaries (Nielsen-Gammon 2002). The strength of the circulation depends on the diurnal heating, i.e., diurnal amplitude of the temperature difference from day to night. Therefore it is an effective approach for evaluation of model per-

formance at local scale to compare modeled diurnal heating against the observed. Diurnal heating can be expressed by diurnal cycle intensity (DCI), defined as the difference between daily maximum and minimum near-surface air temperatures in this study.

The scatterplot of the modeled DCI using different PBL and LSM schemes and the observed DCI from 8 sites during 7–19 May 2001 is shown in Fig. 4. Except for EtaNOAH and MRFNOAH schemes, all other schemes underestimate DCI with the range of MBE from -1.8 to -0.9 °C. EtaNOAH scheme reproduces DCI fairly well, while MRFNOAH scheme overestimates DCI by 1.3 °C. All statistical parameters show that

ACMPX scheme clearly underestimates DCI, especially in the case of high observed DCI, and has the worst performance in predicting DCI overall. This is partly because that ACMPX tends to overestimate minimum temperature (Table 6).

As also seen from Table 6, BLKSLAB, EtaSLAB, and MRFSLAB schemes underestimate maximum temperatures, but overestimate minimum temperatures, which consequently results in relatively small DCIs when compared to the observed. In contrast, EtaNOAH underestimates both maximum temperature and minimum temperature by similar amplitude, which offset each other. Consequently, the error of DCI is very small. For MRFNOAH scheme, it has a small

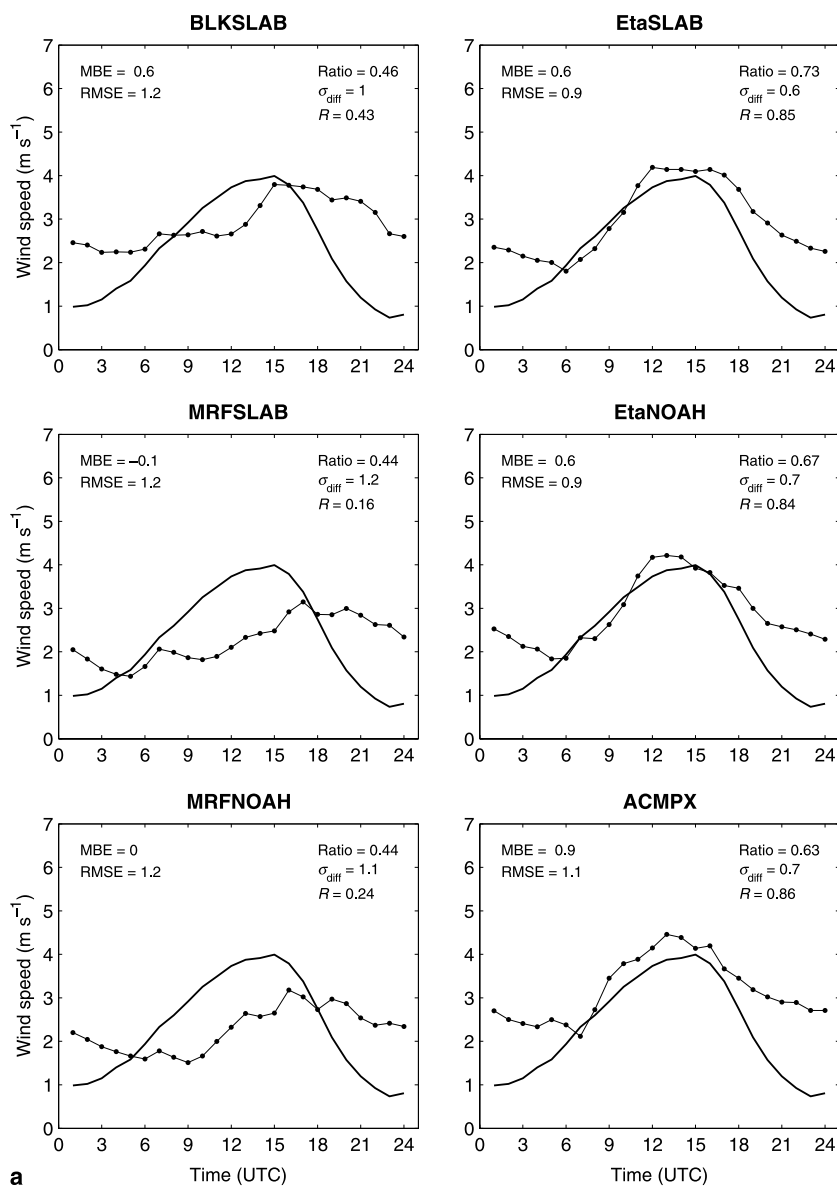


Fig. 6. Observed and modeled diurnal cycle of near-surface wind speed averaged spatially over 12 sites (cf. Table 2) for first week (a) and second week (b). Observed diurnal cycle (solid thick line) is included in each plot for comparison. Diurnal cycle is based on the mean of hourly data for 7–12 May (the first week) and for 13–19 May (the second week), respectively. The statistical parameters are presented within the plot. See the notes of Fig. 5 for weather conditions for the first and second weeks

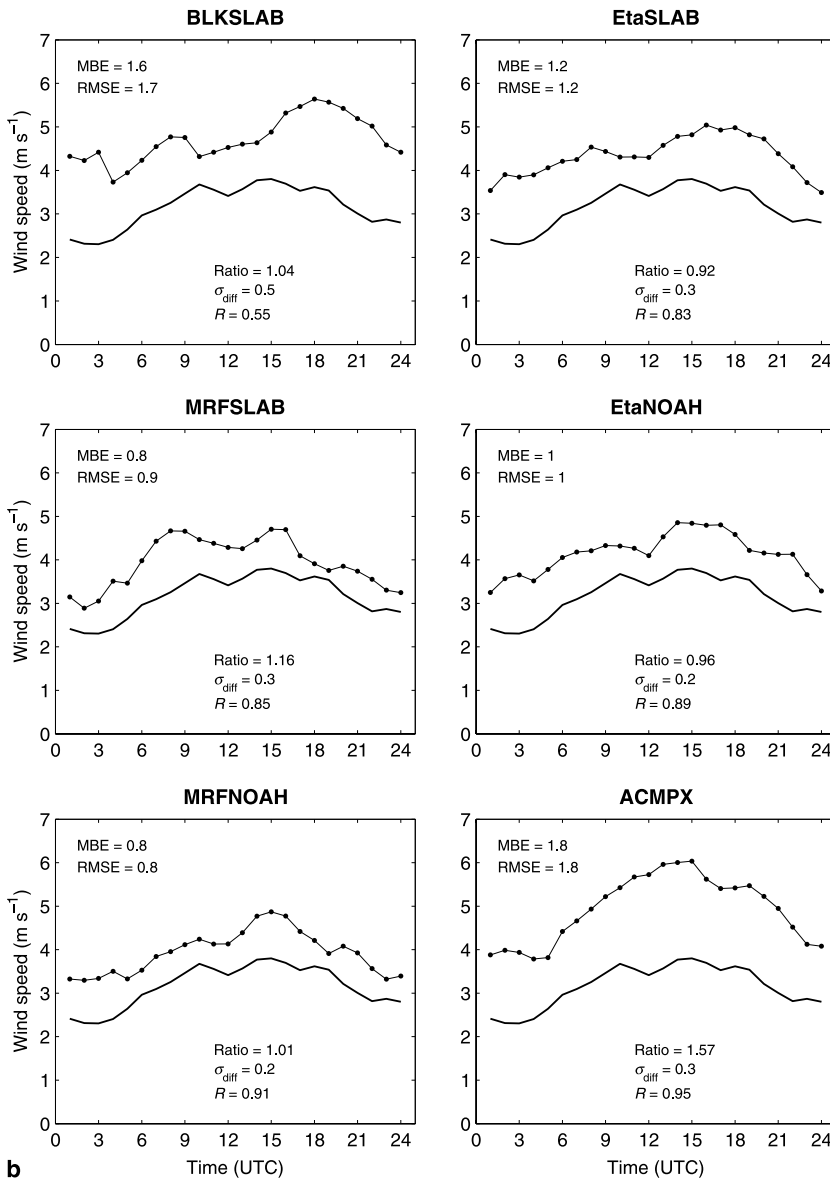


Fig. 6 (continued)

cold bias (-0.1°C) for the maximum temperatures, and a relatively big cold bias (-1.3°C) for the minimum temperature. As a result, the error of DCI is mainly due to the underestimate of the minimum temperature.

It is also noted that the DCI is expected to be affected by cloud cover. The computed correlation coefficient between observed daily mean cloud cover and daily DCI at Säve site (-0.87) implies that there is a negative relationship between cloud cover and DCI. This means that when cloud cover increases the DCI might decrease, and when cloud cover decreases the DCI might increase. Therefore, the error of global radiation caused by random cloud might partly contribute to the error of DCI (cf. Fig. 3 and Table 4).

The averaged diurnal cycles of modeled and observed near-surface air temperature for the two periods are shown in Fig. 5, in which the statistical parameters can be used to evaluate the amplitude and phase of the diurnal cycle (Taylor 2001), as well as the systematic and nonsystematic errors (Zhong et al. 2005). In general, the model using different PBL and LSM schemes reproduces the mean diurnal cycle quite well, especially under fair weather conditions (Fig. 5a). All schemes but ACMPX systematically underestimate the near-surface air temperature for the first week, as indicated by MBE. BLKSLAB, EtaSLAB, and MRFSLAB schemes underestimate the amplitude of diurnal cycle, while EtaNOAH and MRFNOAH schemes estimate it quite well, as re-

vealed by σ_{diff} and ratio. All schemes simulate the phase of diurnal cycle well, as implied by high value of R . ACPMX scheme is evidently different from other schemes in predicting the amplitude and phase of diurnal cycle. It shows the quite good performance during the daytime, but the worse performance during the nighttime hours. For the diurnal cycle of near-surface air temperature averaged over the second week (Fig. 5b), it is different from that over the first week in the amplitude and phase for both the modeled and the observed. In general, all schemes underestimate the amplitudes of diurnal cycle, but simulate the phase fairly well.

Diurnal wind is in response to the diurnal heating cycle. The model performance in simulating the diurnal variation of wind speed is evaluated

by comparing the modeled diurnal cycle with the observed, as shown in Fig. 6. In comparison with the diurnal cycle of near-surface air temperature, the modeled diurnal cycle of near-surface wind speed shows large difference among different PBL and LSM schemes.

The modeled and observed diurnal cycle of wind speed is strong for the first week (Fig. 6a), while it is weak for the second week (Fig. 6b). Local circulation dominates during fair weather (the first week), but influences from synoptic scale weather play a dominate role for the second week. For the first week, there is large discrepancy between the modeled and observed diurnal cycles for all PBL and LSM schemes. In comparison, BLKSLAB, MRFSLAB and MRFNOAH schemes simulate the amplitude and phase of

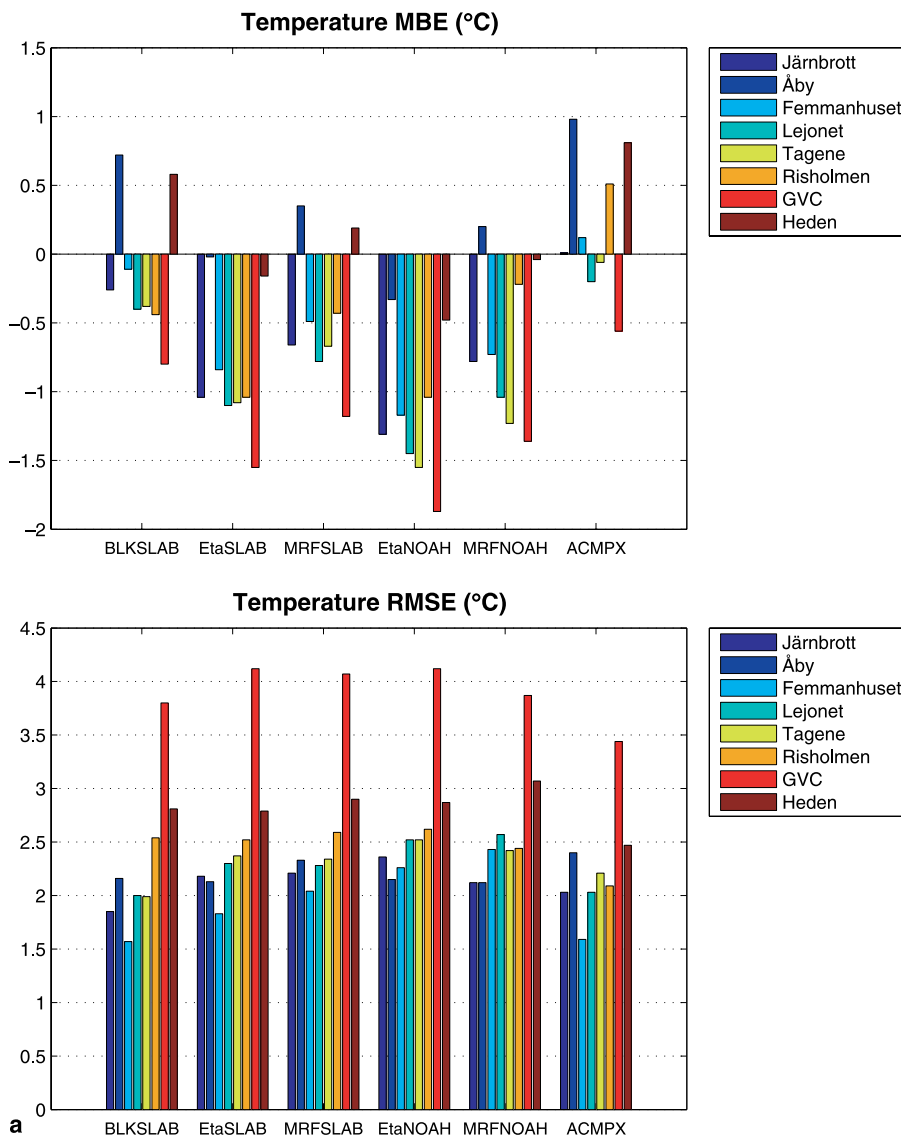


Fig. 7. Statistical measures of near-surface air temperature (a) and near-surface wind speed (b) with different experiment schemes for each observational site. For temperature, 8 sites are involved (same as in Fig. 5), while 12 sites are involved for wind speed (same as in Fig. 6). Top: MBE, bottom: RMSE

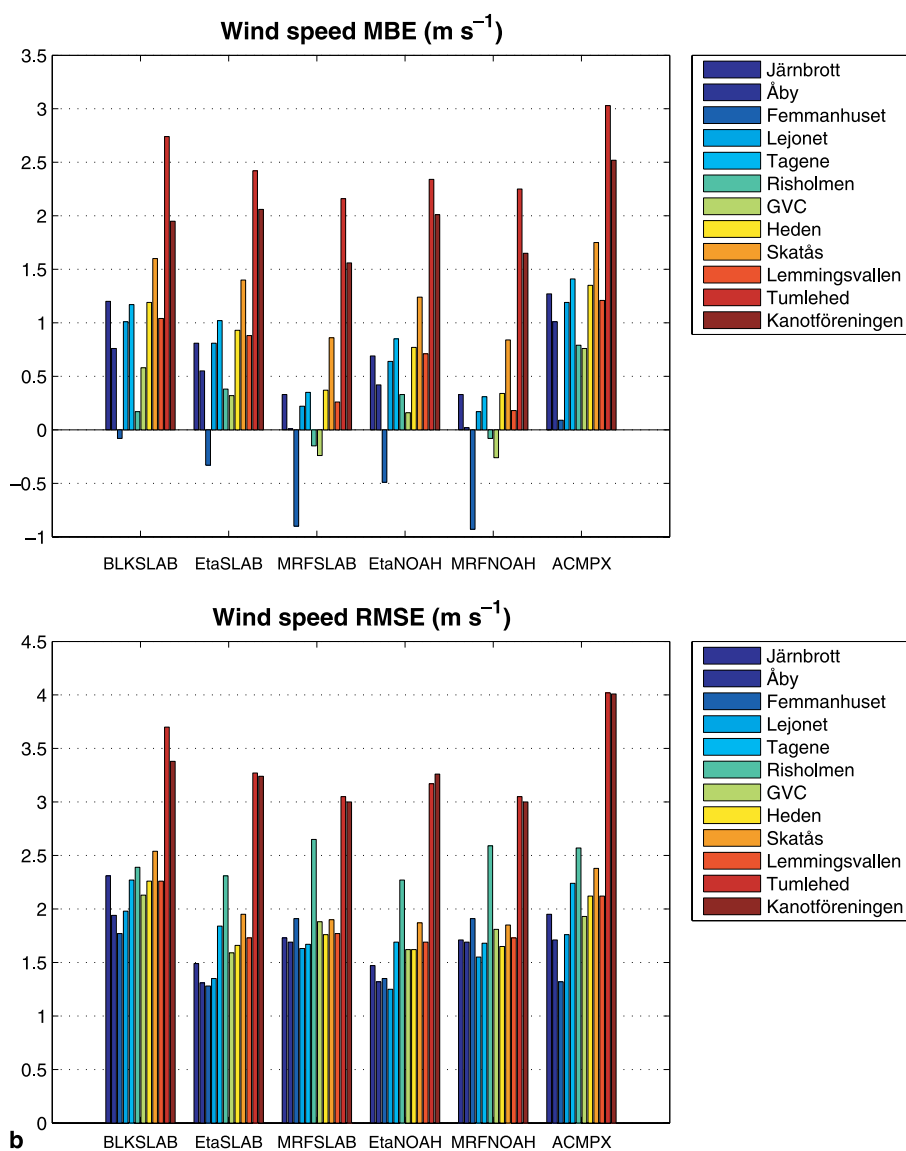


Fig. 7 (continued)

wind diurnal cycle worse, whereas EtaSLAB, EtaNOAH and ACPX schemes simulate them fairly well, in particular during the daytime. Also, wind speeds are always overestimated during the nighttime for all schemes. For the second week, all schemes estimate the amplitude and phase of wind diurnal cycle well in statistical sense, but have large fluctuations in wind speed diurnal variation.

Some similar results on diurnal cycles of surface temperatures and winds under clear skies can be found in Zhang and Zheng (2004).

4.3 Spatial differences

To investigate whether the model forecast errors using different PBL and LSM schemes depend on

the locations of the sites, statistical measures of hourly near-surface air temperature and wind are computed over temporal domain for each site, respectively.

As an example, Fig. 7 presents the MBE and RMSE of near-surface air temperature and wind speed, respectively. For the temperature, the difference among the stations for each scheme and the difference among different schemes for each site do exist. At the GVC site, where the temperature was measured over the building roof, the difference between observed and modeled results is statistically significant at the 95% confidence level (T-test) for all schemes but ACPX. For the wind speed, the difference among the stations for each scheme exists, and is more evident for all schemes at the Tumlehed and

Kanotföreningen sites, which are close to the coastline.

4.4 Boundary-layer structure

4.4.1 Vertical temperature gradient and nocturnal inversion

The stability of lower atmosphere is characterized by vertical temperature gradient, which is often measured from instrumental mast. In this study, the vertical temperature gradient between 3 and 105 m at the Järnbrott mast site is used to compare with the modeled results, as seen in Fig. 8. On the whole, all schemes but

MRFNOAH underestimate the temperature gradients by 0.5–1.1 °C per 100 m. Among all schemes, EtaNOAH and MRFNOAH show the best performance in predicting the vertical temperature gradients, as indicated by all statistical parameters, compared to other schemes. Clearly, ACMPX scheme underestimates them.

To further understand these differences resulted from using different PBL and LSM schemes, it is worthy showing their performance estimating the near-surface and lower level temperatures, respectively (Fig. 9). All schemes underestimate both the near-surface air temperature (Fig. 9a) and the lower-level temperature (Fig. 9b) in statistical sense. The errors offset each other when

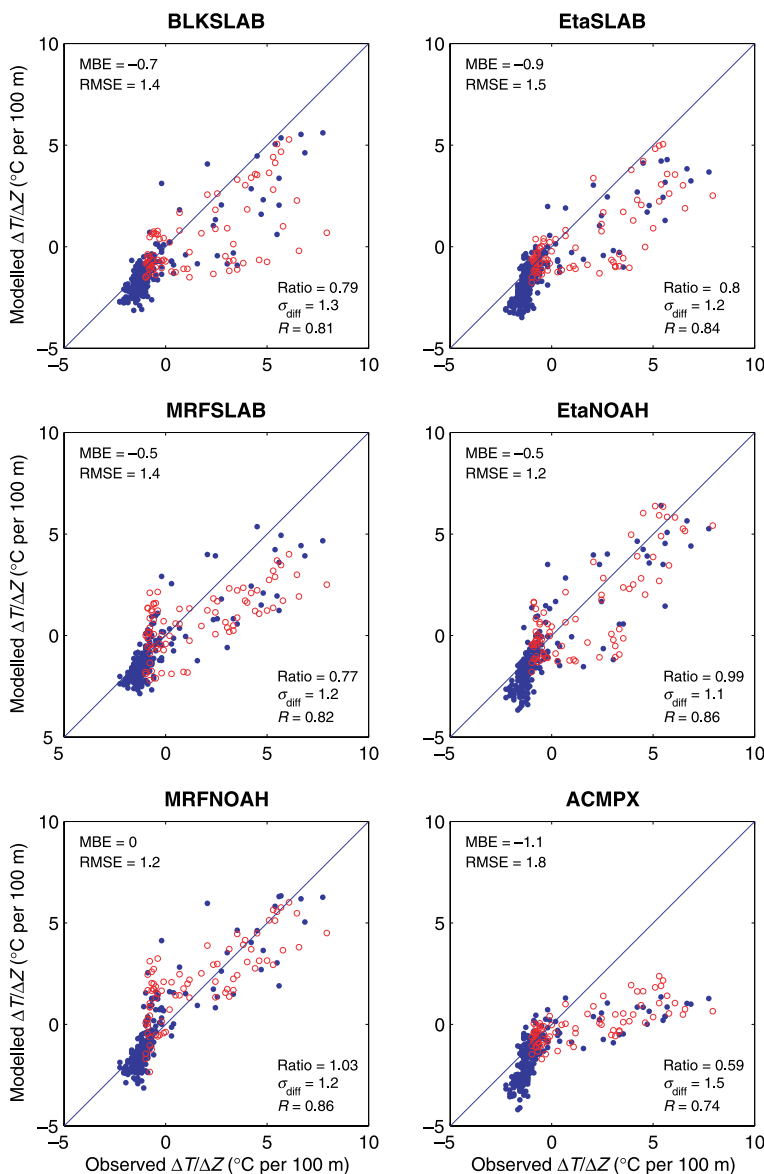


Fig. 8. Observed and modeled vertical temperature gradient with different experiment schemes at Järnbrott mast site. The results are based on hourly data of near-surface and 105-m measurements/simulations during the period from 7–19 May 2001 (sample number $N = 311$). The statistical parameters are presented within the plot. The temperature gradient during night hours is denoted by open circle to show nocturnal temperature inversion for clarity

estimating the vertical temperature gradient. Interestingly, all schemes show a good agreement of the rise and fall tendency of temperature with the observations. This implies that the timing of vertical temperature gradients is reproduced well.

Surface-based inversion strength at night is a key meteorological factor for air quality applications, which governs vertical mixing of near-surface pollutants. The nocturnal temperature inversion is used to measure the surface-based inversion strength at night. Based on the hourly nighttime vertical temperature gradient at the Järbrott mast site, Table 8 summarizes the occurrence hours of nocturnal temperature inversion indicated by observed and modeled results

during the GÖTE2001 period, as well as mean inversion strength. The results show that Eta-NOAH and MRFNOAH schemes predict comparable temperature inversion strength, whereas other schemes generally underestimate it by 2–3 °C per 100 m. Additionally, in comparison with the observed potential temperature inversion within the lowest 200 m at midnight from the radiosoundings available at Landvetter airport site (Table 9), all schemes show similar results to those from the Järbrott mast site (Table 8). Some findings are consistent with those from several previous studies using similar PBL and LSM schemes (e.g., Hanna and Yang 2001; Zhong and Fast 2003; Zhong et al. 2005).

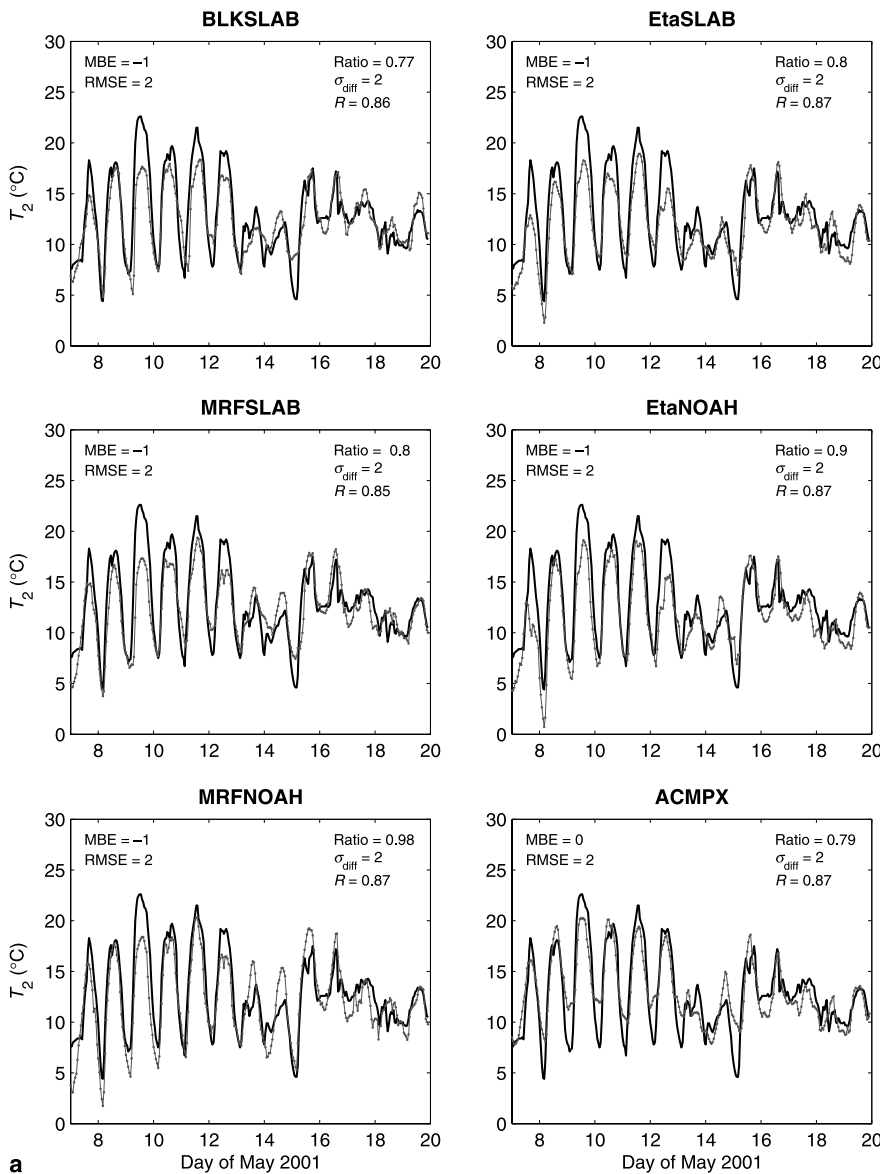


Fig. 9. Hourly variation of near-surface air temperature (a) and 105-m temperature (b) modeled by different experiment schemes during the period from 0000 UTC 7 May to 2200 UTC 20 May 2001 (sample number $N=311$) at the closest grid point to Järbrott mast site. Observed near-surface and 105-m temperatures at Järbrott mast site are denoted by thick solid line in (a) and (b), respectively, within each plot. The statistical measures are presented within the plot

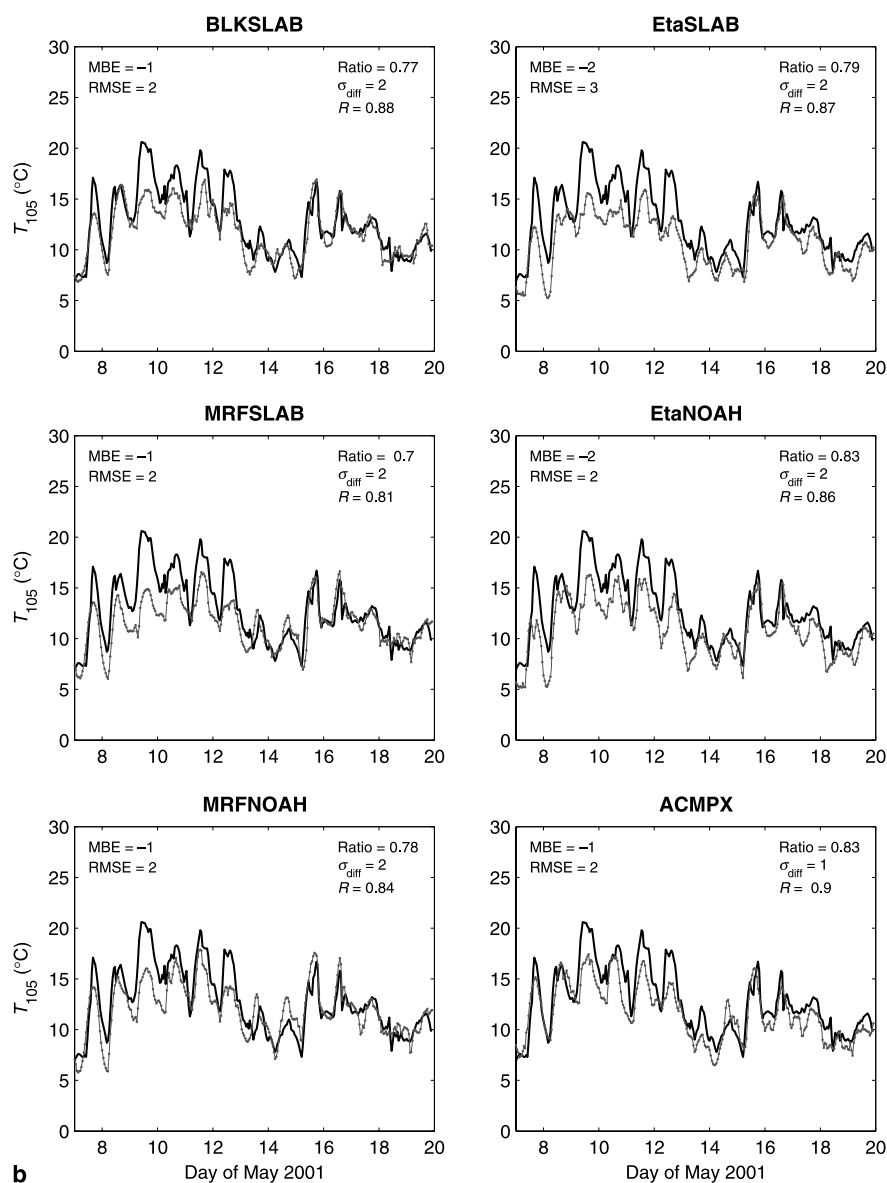


Fig. 9 (continued)

Table 8. Occurrence (hours) and mean strength of nocturnal temperature inversion (NTinv) revealed by observed and modeled results at Järnbrott site during the GÖTE2001 period

Parameter ^a	Obs	BLKSLAB	EtaSLAB	MRFSLAB	EtaNOAH	MRFNOAH	ACMPX
Occurrence ^b	42	35	30	56	41	66	32
Strength ^c	3.5	1.2	1.1	1.3	2.2	3.2	0.5
Strength ^d	3.5	2.0	2.1	1.4	2.7	2.6	0.9

^a Based on hourly data for nighttime during the period of 7–19 May 2001 at Järnbrott (mast) site (sample number: 79)

^b When the temperature difference between 105-m and near-surface is greater than 0.0 °C

^c Averaged over the period corresponding to the occurrence of observed NTinv (unit: °C per 100 m)

^d Averaged over the period for the occurrence of observed and modeled NTinv (unit: °C per 100 m), respectively

4.4.2 PBL height

PBL height, or turbulent mixing depth, as an input variable to air quality models, is critical to vertical

transport of pollutants, horizontal plume dispersion and dry deposition in the PBL (Seaman 2000; Angevine and Mitchell 2001; Mao et al. 2006).

Table 9. Observed and modeled surface-based potential temperature inversion within the lowest 200 m at midnight (0000 UTC) at Landvetter site during the period from 7 to 17 May 2001 (unit: K per 100 m), as well as some statistical parameters

Date/statistics	Obs ^a	BLKSLAB	EtaSLAB	MRFSLAB	EtaNOAH	MRFNOAH	ACMPX
7	1.1	1.0	0.9	1.4	1.6	2.0	0.6
8	2.6	1.7	1.7	1.4	2.8	2.5	1.0
9	4.3	2.9	2.5	2.6	3.8	4.1	1.5
10	3.8	2.4	2.4	2.2	3.5	3.2	1.9
11	3.9	1.3	1.9	1.2	3.3	2.6	1.5
12	3.4	1.7	1.9	2.1	3.0	3.0	0.8
13	2.7	1.1	0.3	0.8	1.1	2.1	1.1
14	1.3	0.2	0.0	0.2	0.1	1.7	0.2
15	1.9	0.3	0.2	2.3	1.0	3.7	0.6
16	1.1	0.0	0.1	0.2	0.0	0.6	0.2
17	0.6	0.7	0.3	1.2	0.4	2.0	0.3
Mean	2.4	1.2	1.1	1.4	1.9	2.5	0.9
MBE		-1.2	-1.3	-1.0	-0.6	0.1	-1.5
RMSE		1.5	1.5	1.5	0.8	0.9	1.8
σ_{diff}		0.7	0.7	1.0	0.6	0.9	0.8
Ratio		0.70	0.75	0.62	1.10	0.75	0.44
R		0.82	0.86	0.60	0.90	0.69	0.90

^a Observed data is from radiosounding (RAOB) at Landvetter (airport) site

Table 10. PBL height (m) estimated from modeled and observed results at noon (1200 UTC) at Landvetter site during the period from 7 to 16 May 2001

Date/statistics	Obs ^a	BLKSLAB	EtaSLAB	MRFSLAB	EtaNOAH	MRFNOAH	ACMPX
7	1023	776	1142	1298	1144	1425	1329
8	1267	1128	976	1140	986	1300	1245
9	1785	1397	965	1238	992	1385	1415
10	292	1155	579	1276	714	1152	1200
11	918	1305	1124	1434	933	1315	1323
12	1226	972	262	749	96	1323	1345
13	432	476	299	585	315	808	694
14	704	542	372	641	374	1059	466
15	1413	807	678	1163	631	1558	787
16	1851	966	585	1875	683	1839	1114
Mean	1091	952	698	1140	687	1316	1092
MBE		-139	-393	49	-404	225	1
RMSE		513	675	465	689	410	505
Ratio		0.58	0.64	0.75	0.65	0.53	0.62
R		0.39	0.29	0.52	0.27	0.82	0.37

^a PBL height for radiosounding (RAOB) data is estimated based on maximum potential temperature gradient (capping inversion zone) (cf. Seibert et al. 2000)

To evaluate how well all the PBL and LSM schemes capture the daytime PBL height, and to compare the difference among these schemes, the diagnosed PBL heights in the model using different PBL and LSM schemes are compared to the observed ones from all radiosoundings available at the Landvetter site at noon (midday) during the GÖTE2001 period (Table 10). The predicted PBL heights show noticeable difference among

different PBL and LSM schemes. Statistically, BLKSLAB, EtaSLAB, EtaNOAH schemes underestimate the observed PBL heights by 13, 36, and 37%, respectively, while MRFSLAB and MRFNOAH schemes overestimate by 4 and 21%, respectively. ACMPX shows a little bias. However, all schemes underestimate the variability of PBL heights, and have RMSE of 400–700 m. Among all schemes, MRFSLAB and MRFNOAH

display relatively good performance in predicting PBL heights. The results indicate that the model predicted PBL height is sensitive to PBL and LSM schemes.

Several previous studies also reported the model performance in predicting PBL heights. For example, Zhong et al. (2005) reported that the predicted PBL heights using EtaSLAB scheme are substantially lower than the observed. Berg and Zhong (2005) showed that MRFSLAB scheme consistently overestimates the PBL heights, while BLKSLAB has good agreement with the observed PBL height (also see Hanna and Yang 2001). These findings are consistent with the results using similar PBL and LSM schemes in this study.

4.4.3 Low-level jet

Low-level jet (LLJ) is a prominent feature within the PBL. It plays an important role in the transport of water vapor and pollutants (Athanasiadis et al. 2002; Mao and Talbot 2004). During the GÖTE2001 field campaign, a strong LLJ was observed from Landvetter radiosoundings at midnight of 7 and 8 May 2001, respectively. To reveal the ability of the model in simulating LLJs using different PBL and LSM schemes, Fig. 10 shows the observed and modeled vertical profiles of wind speed and wind direction within the 3 km, and some observed and modeled LLJ characteristic parameters are presented in Table 11.

All schemes reasonably simulate the occurrence height of nocturnal LLJ of 7 May, but underesti-

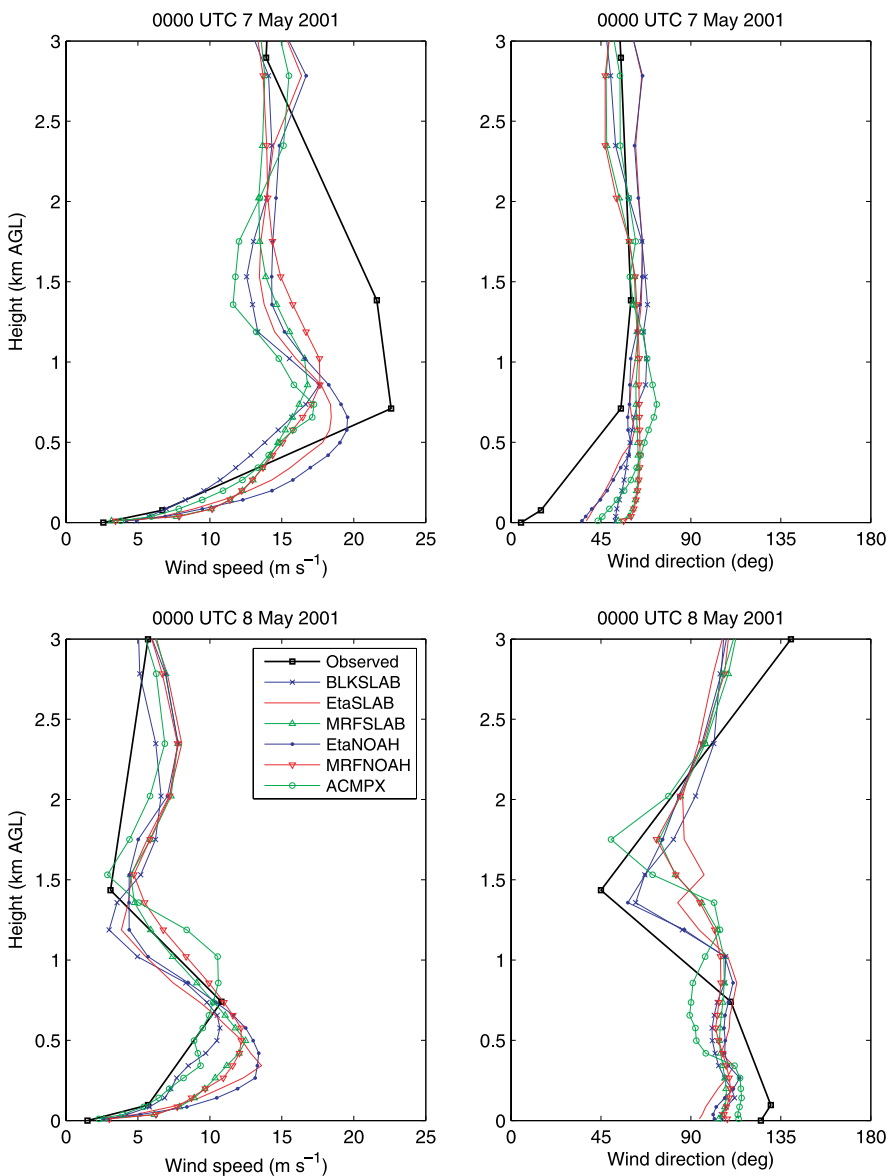


Fig. 10. Observed and modeled vertical profiles of wind speed (left) and wind direction (right) with different experiment schemes within 3 km showing low-level jet (LLJ) at Landvetter radiosounding site at 0000 UTC 7 May 2001 (top), and 0000 UTC 8 May 2001 (bottom)

Table 11. Characteristic parameters of observed and modeled LLJs at midnight (0000 UTC) at Landvetter site by different experiment schemes^a on selected days during the GÖTE2001 period

Date ^b	Characteristic parameters ^c	OBS	BS	ES	MS	EN	MN	AP
7	WS _{Max}	22.6	17.6	18.4	16.8	19.6	17.6	17.2
	H	710	857	656	857	656	857	736
	WD _{Diff}	55°	16°	28°	10°	30°	8°	29°
8	WS _{Max}	10.8	10.7	13.6	12.5	13.4	12.2	10.6
	H	740	576	342	498	420	498	857
	WD _{Diff}	85°	50°	30°	34°	56°	37°	65°

^a Abbreviation for experiment scheme name: Same as in Table 4. OBS: Observed

^b Selected according to Hsu (1988, pp. 155–162)

^c WS_{Max}: Low-level wind maxima (m s^{-1}), H: Height for low-level wind maxima (m), WD_{Diff}: Maximum change in wind direction (degree) with height within PBL (2000 m)

mate its strength (i.e., maximum wind speed) by $3\text{--}6 \text{ m s}^{-1}$. In contrast, these schemes reasonably simulate the LLJ strength of 8 May, but underestimate its occurrence height. Also, some differences in predicting the LLJs exist among the schemes. For example, EtaNOAH simulates LLJ strength best on 7 May, but worse on 8 May. ACMPX simulates LLJ strength of 7 May worse, but LLJ of 8 May better. The difference between observed and modeled LLJs (strength and occurrence height) is partly due to the coarse resolution for RAOB observation compared to model vertical resolutions within the PBL. Also, the difference between the actual elevation for observation and model terrain elevation likely causes some difference in the LLJ occurrence height between the observed and modeled.

5. Conclusions and remarks

This study evaluates the performance of MM5 Version 3.6.3 using different PBL and LSM parameterizations at local scale over the Swedish west coast, and compares the differences in the performance. Some schemes have been evaluated in previous studies (BLKSLAB, EtaSLAB and MRFSLAB), while the others (EtaNOAH, MRFNOAH and ACMPX) are less evaluated. Therefore, the findings about the model performance using EtaNOAH, MRFNOAH and ACMPX schemes in this study are quite new. The main conclusions of the study are as follows:

(1) For near-surface air temperature, BLKSLAB, EtaSLAB and MRFSLAB schemes have an overall cold bias of less than 1.0°C , a cold bias of 0.4 to 1.2°C during the daytime, and a slightly warm bias during the nighttime;

EtaNOAH and MRFNOAH schemes have consistently cold biases during day and night; ACMPX scheme has a small cold bias (-0.1°C) during the daytime, but a warm bias of 1.1°C during the nighttime, yielding an overall warm bias of 0.2°C . BLKSLAB, EtaSLAB, and MRFSLAB schemes underestimate maximum temperature, but slightly overestimate minimum temperature. EtaNOAH and MRFNOAH schemes underestimate both maximum and minimum temperatures. ACMPX slightly underestimates maximum temperature, but overestimates minimum temperatures with a warm bias of 1.7°C . Consequently, BLKSLAB, EtaSLAB, MRFSLAB, and ACMPX schemes have a negative bias of DCI from -1.8 to -0.9°C . EtaNOAH scheme predicts the observed DCI reasonably well, while MRFNOAH overestimates DCI by 1.3°C . All schemes but ACMPX underestimate the temperature by $1.0\text{--}2.3^\circ\text{C}$ under the fair weather conditions (the first week), but have a small bias ranging from -0.2 to 0.7°C under the cloudy or rainy conditions (the second week). ACMPX scheme displays a slightly warm bias (0.2°C) during both the first week and the second week.

(2) For near-surface wind speed, all schemes overestimate it with a range of bias from 0.4 to 1.4 m s^{-1} overall. The biases are smaller during the daytime than during the nighttime for all schemes. Under fair weather conditions, BLKSLAB, EtaSLAB, EtaNOAH and ACMPX schemes show a positive bias of less than 1.0 m s^{-1} , while MRFSLAB and MRFNOAH schemes have

a slightly negative bias (-0.1 m s^{-1}); Under the cloudy or rainy conditions, all schemes display a relative large positive bias, ranging from 0.8 to 1.8 m s^{-1} .

- (3) All schemes capture the diurnal cycle of near-surface temperature and wind speed to different extent during the first week and the second week. The modeled amplitude and phase varies evidently from scheme to scheme. Also, the variation depends on weather conditions.
- (4) All schemes can capture presence of nocturnal temperature inversion to some extent. However, BLKSLAB, EtaSLAB, MRFSLAB, and ACMPX schemes underestimate its intensity, especially ACMPX scheme. By comparison, EtaNOAH and MRFNOAH schemes simulate nocturnal temperature inversion reasonably well.
- (5) BLKSLAB, EtaSLAB, and EtaNOAH schemes underestimate PBL heights (at mid-day only), while MRFSLAB and MRFNOAH schemes overestimate PBL heights. ACMPX scheme displays the best performance in predicting the PBL heights in statistical sense. It is clear that MRF PBL scheme tends to overestimate PBL heights, while Eta PBL scheme tends to underestimate PBL heights.
- (6) All schemes underestimate the strength of nocturnal LLJ of 7 May 2001 by $3\text{--}6 \text{ m s}^{-1}$, but simulate the LLJ strength of 8 May reasonably well.

In summary, using different PBL and LSM schemes in MM5 exhibits different performance. The difference depends on the simulated variables, time of a day, and synoptic weather conditions. The model performance in predicting global radiation, diurnal cycle of near-surface air temperature and wind speed, diurnal cycle intensity, vertical temperature gradient, nocturnal temperature inversion and PBL heights, which are critical parameters for air quality applications, depends to a larger extent on PBL and LSM parameterizations. Therefore, choosing PBL and LSM schemes is important for applications of MM5 in air quality modeling. Moreover, using advanced/complicated LSM schemes (e.g., Noah and PX LSMs) does not mean that they can present good results as compared to using simple SLAB model. Further investigation of influence of PBL and LSM parameterizations under dif-

ferent seasons and climate regimes at various scales is desirable for evaluating MM5 model performance.

At last, as a remark, it is necessary to notice that the screen height in ACMPX scheme is 1.5 m , compared to 2.0 m in all other schemes. Additional numerical analyses show that typically the difference between the temperatures at 1.5 m and 2.0 m , $T_{1.5 \text{ m}} - T_{2.0 \text{ m}}$, is around -1.0°C during daytime and 0.5°C during nighttime. In this study, however, no effort has been made to correct this difference. Thus, interpretation and application of the statistics for that scheme need to take this effect into consideration.

Acknowledgments

The Faculty of Science at Göteborg University and Adlersbergska Stipendiefonden are thanked for their support to Junfeng Miao. This work was also supported by Wilhelm and Martina Lundgren Science Fund as a project *Air Pollution Dynamics: 3-D Meteorological Modelling for Air Quality Studies over the Swedish West Coast* to Junfeng Miao. The Swedish Research Council is thanked for its support to Deliang Chen. Moreover, the authors greatly appreciate two anonymous reviewers for their valuable comments and constructive suggestions to improve the manuscript.

References

- Angevine WM, Mitchell K (2001) Evaluation of the NCEP mesoscale Eta model convective boundary layer for air quality applications. *Mon Wea Rev* 129: 2761–75
- Athanassiadis GA, Rao ST, Ku JY, Clark RD (2002) Boundary layer evolution and its influence on ground-level ozone concentrations. *Environ Fluid Mech* 2: 339–57
- Barna M, Lamb B, O'Neill S, Westberg H, Figueroa-Kaminsky C, Otterson S, Bowman C, DeMay J (2000) Modeling ozone formation and transport in the Cascadia region of the Pacific Northwest. *J Appl Meteor* 39: 349–66
- Berg LK, Zhong SY (2005) Sensitivity of MM5-simulated boundary layer characteristics to turbulence parameterizations. *J Appl Meteor* 44: 1467–83
- Betts AK, Chen F, Mitchell KE, Janjić ZI (1997) Assessment of the land surface and boundary layer models in two operational versions of the NCEP Eta model using FIFE data. *Mon Wea Rev* 125: 2896–916
- Blackadar AK (1976) Modeling the nocturnal boundary layer. Preprints of 3rd Symp. on Atmospheric Turbulence, Diffusion and Air Quality, American Meteorological Society, Raleigh, NC
- Blackadar AK (1979) High resolution models of the planetary boundary layer. In: Pfafflin J, Ziegler E (eds.) *Advances in environmental science and engineering*, Vol. 1, No. 1. Gordon and Breach Science Publishers, Newark, pp. 50–85

- Borne K, Chen D, Miao J-F, Achberger C, Lindgren J, Hallquist M, Pettersson J, Haeger-Eugensson M, Wyser K, Eliasson I, Langner J (2005) Data report on measurements of meteorological- and air pollution variables during the campaign GÖTE-2001. Research Report C67, Earth Sciences Centre, Göteborg University, Göteborg, Sweden, 28 pp
- Braun SA, Tao WK (2000) Sensitivity of high-resolution simulations of hurricane Bob (1991) to planetary boundary layer parameterizations. *Mon Wea Rev* 128: 3941–61
- Bright DR, Mullen SL (2002) The sensitivity of the numerical simulation of the southwest monsoon boundary layer to the choice of PBL turbulence parameterization in MM5. *Wea Forecast* 17: 99–114
- Case JL, Manobianco J, Dianic AV, Wheeler MW, Harms DE, Parks CR (2002) Verification of high-resolution RAMS forecasts over East-Central Florida during the 1999 and 2000 summer months. *Wea Forecast* 17: 1133–51
- Chandrasekar A, Philbrick CR, Clark R, Doddridge B, Georgopoulos P (2003) Evaluating the performance of a computationally efficient MM5/CALMET system for developing wind field inputs to air quality models. *Atmos Environ* 37: 3267–76
- Chen F, Dudhia J (2001a) Coupling an advanced land surface-hydrology model with the Penn State-NCAR MM5 modeling system: Part I – model implementation and sensitivity. *Mon Wea Rev* 129: 569–85
- Chen F, Dudhia J (2001b) Coupling an advanced land surface-hydrology model with the Penn State-NCAR MM5 modeling system: Part II – preliminary model validation. *Mon Wea Rev* 129: 587–604
- Cheng WYY, Steenburgh WJ (2005) Evaluation of surface sensible weather forecasts by the WRF and the Eta models over the western United States. *Wea Forecast* 20: 812–21
- Cox R, Bauer BL, Smith T (1998) A mesoscale model intercomparison. *Bull Amer Meteor Soc* 79: 265–83
- Dudhia J (1989) Numerical study of convection observed during the Winter Monsoon Experiment using a mesoscale two-dimensional model. *J Atmos Sci* 46: 3077–107
- Dudhia J (1996) A multi-layer soil temperature model for MM5. Sixth Annual PSU/NCAR Mesoscale Model Users' Workshop, Boulder, CO, July 1996
- Fan HL, Sailor DJ (2005) Modeling the impacts of anthropogenic heating on the urban climate of Philadelphia: a comparison of implementations in two PBL schemes. *Atmos Environ* 39: 73–84
- Grell GA, Dudhia J, Stauffer DR (1995) A description of the fifth-generation Penn State/NCAR Mesoscale Model (MM5). NCAR Technical Note, NCAR/TN-398 + STR, National Center for Atmospheric Research, Boulder, CO, 122 pp
- Grell GA, Emeis S, Stockwell WR, Schoenemeyer T, Forkel R, Michalakes J, Knoche R, Seidl W (2000) Application of a multiscale, coupled MM5/chemistry model to the complex terrain of the VOTALP valley campaign. *Atmos Environ* 34: 1435–53
- Hanna SR, Yang RX (2001) Evaluations of mesoscale models' simulations of near-surface winds, temperature gradients, and mixing depths. *J Appl Meteor* 40: 1095–104
- Hogrefe C, Rao ST, Kasibhatla P, Kallos G, Tremback CJ, Hao W, Olerud D, Xiu A, McHenry J, Alapaty K (2001) Evaluating the performance of regional-scale photochemical modeling systems: Part I – meteorological predictions. *Atmos Environ* 35: 4159–74
- Hong SY, Pan HL (1996) Nonlocal boundary layer vertical diffusion in a medium-range forecast model. *Mon Wea Rev* 124: 2322–39
- Hsu SA (1988) Coastal meteorology. New York: Academic Press, 260 pp
- Jackson B, Chau D, Gurer K, Kaduwela A (2006) Comparison of ozone simulations using MM5 and CALMET/MM5 hybrid meteorological fields for the July/August 2000 CCOS episode. *Atmos Environ* 40: 2812–22
- Janjić ZI (1990) The step-mountain coordinate: physical package. *Mon Wea Rev* 118: 1429–43
- Janjić ZI (1994) The step-mountain Eta coordinate model: further developments of the convection, viscous sub-layer, and turbulence closure schemes. *Mon Wea Rev* 122: 927–45
- Kain JS (2004) The Kain–Fritsch convective parameterization: an update. *J Appl Meteor* 43: 170–81
- Kotroni V, Lagouvardos K (2001) Precipitation forecast skill of different convective parameterization and microphysical schemes: application for the cold season over Greece. *Geophys Res Lett* 28: 1977–80
- Kotroni V, Lagouvardos K (2004) Evaluation of MM5 high-resolution real-time forecasts over the urban area of Athens, Greece. *J Appl Meteor* 43: 1666–78
- Ku JY, Mao H, Zhang K, Civerolo K, Rao ST, Philbrick CR, Doddridge B, Clark R (2001) Numerical investigation of the effects of boundary-layer evolution on the predictions of ozone and the efficacy of emission control options in the northeastern United States. *Environ Fluid Mech* 1: 209–33
- Lee SM, Fernando HJS (2004) Evaluation of meteorological models MM5 and HOTMAC using PAFEX-I data. *J Appl Meteor* 43: 1133–48
- Manabe S (1969) Climate and the ocean circulation – I. The atmospheric circulation and the hydrology of the Earth's surface. *Mon Wea Rev* 97: 739–74
- Mandal M, Mohanty UC, Raman S (2004) A study on the impact of parameterization of physical processes on prediction of tropical cyclones over the Bay of Bengal with NCAR/PSU mesoscale model. *Nat Hazards* 31: 391–414
- Mao H, Talbot R (2004) Role of meteorological processes in two New England ozone episodes during summer 2001. *J Geophys Res* 109: D20305 (DOI: 10.1029/2004JD004850)
- Mao Q, Gautney LL, Cook TM, Jacobs ME, Smith SN, Kelsoe JJ (2006) Numerical experiments on MM5-CMAQ sensitivity to various PBL schemes. *Atmos Environ* 40: 3092–110
- Mellor GL, Yamada T (1974) A hierarchy of turbulence closure models for planetary boundary layers. *J Atmos Sci* 31: 1791–806

- Miao J-F (2006) Meteorological modelling in coastal areas – local climate and air quality. Ph.D. thesis, A107, Earth Sciences Centre, Göteborg University, Göteborg, Sweden, 190 pp
- Miao J-F, Chen D, Wyser K (2006) Modelling subgrid scale dry deposition velocity of O₃ over the Swedish west coast with MM5-PX model. *Atmos Environ* 40: 415–29
- Mlawer EJ, Taubman SJ, Brown PD, Iacono MJ, Clough SA (1997) Radiative transfer for inhomogeneous atmospheres: RRTM, a validated correlated-K model for the longwave. *J Geophys Res* 102(D14): 16663–82
- Nielsen-Gammon JW (2002) Validation of physical processes in MM5 for photochemical model input: The Houston 2000 ozone episode. Preprints of the 12th PSU/ NCAR Mesoscale Model User's Workshop, NCAR, Boulder, CO
- Pérez C, Jiménez P, Jorba O, Sicard M, Baldasano JM (2006) Influence of the PBL scheme on high-resolution photochemical simulations in an urban coastal area over the Western Mediterranean. *Atmos Environ* 40: 5274–97
- Pino D, Vilà-Guerau de Arellano J, Comerón A, Rocadenbosch F (2004) The boundary layer growth in an urban area. *Sci Total Environ* 334–335: 207–13
- Pleim JE, Chang JS (1992) A non-local closure model for vertical mixing in the convective boundary layer. *Atmos Environ* 26A: 965–81
- Pleim JE, Xiu A (1995) Development and testing of a surface flux and planetary boundary layer model for application in mesoscale models. *J Appl Meteor* 34: 16–32
- Rao ST, Ku JY, Berman S, Zhang K, Mao H (2003) Summertime characteristics of the atmospheric boundary layer and relationships to ozone levels over the Eastern United States. *Pure Appl Geophys* 160: 21–55
- Ratnam JV, Kumar KK (2005) Sensitivity of the simulated monsoons of 1987 and 1988 to convective parameterization schemes in MM5. *J Clim* 18: 2724–43
- Seaman NL (2000) Meteorological modeling for air-quality assessments. *Atmos Environ* 34: 2231–59
- Seibert P, Beyrich F, Gryning S-E, Joffre S, Rasmussen A, Tercier P (2000) Review and intercomparison of operational methods for the determination of the mixing height. *Atmos Environ* 34: 1001–27
- Shafran PC, Seaman NL, Gayno GA (2000) Evaluation of numerical predictions of boundary layer structure during the Lake Michigan ozone study. *J Appl Meteor* 39: 412–26
- Sokhi RS, San José R, Kitwiroon N, Fragkou E, Pérez JL, Middleton DR (2006) Prediction of ozone levels in London using the MM5-CMAQ modelling system. *Environ Model Software* 21: 566–76
- Svensson MK, Eliasson I (2002) Diurnal air temperatures in built-up areas in relation to urban planning. *Landscape Urban Plan* 61: 37–54
- Taylor KE (2001) Summarizing multiple aspects of model performance in a single diagram. *J Geophys Res* 106(D7): 7183–92
- Xiu A, Pleim JE (2001) Development of a land surface model: Part I – application in a mesoscale meteorological model. *J Appl Meteor* 40: 192–209
- Xu J, Small EE (2002) Simulating summertime rainfall variability in the North American monsoon region: the influence of convection and radiation parameterizations. *J Geophys Res* 107(D23): 4727 (DOI: 10.1029/2001JD002047)
- Zamora RJ, Solomon S, Dutton EG, Bao JW, Trainer M, Portmann RW, White AB, Nelson DW, McNider RT (2003) Comparing MM5 radiative fluxes with observations gathered during the 1995 and 1999 Nashville southern oxidants studies. *J Geophys Res* 108(D2): 4050 (DOI: 10.1029/2002JD002122)
- Zhang DL, Anthes RA (1982) A high-resolution model of the planetary boundary layer – sensitivity tests and comparisons with SESAME-79 data. *J Appl Meteor* 21: 1594–609
- Zhang DL, Zheng WZ (2004) Diurnal cycles of surface winds and temperatures as simulated by five boundary layer parameterizations. *J Appl Meteor* 43: 157–69
- Zhang K, Mao H, Civerolo K, Berman S, Ku JY, Rao ST, Doddridge B, Philbrick CR, Clark R (2001) Numerical investigation of boundary-layer evolution and nocturnal low-level jets: local versus non-local PBL schemes. *Environ Fluid Mech* 1: 171–208
- Zhong SY, Fast J (2003) An evaluation of the MM5, RAMS, and Meso-Eta models at subkilometer resolution using VTMX field campaign data in the Salt Lake valley. *Mon Wea Rev* 131: 1301–22
- Zhong SY, In HJ, Bian XD, Charney J, Heilman W, Potter B (2005) Evaluation of real-time high-resolution MM5 predictions over the Great Lakes Region. *Wea Forecast* 20: 63–81